

Article

Experimental Performance Comparison of High-Glide Hydrocarbon and Synthetic Refrigerant Mixtures in a High-Temperature Heat Pump

Leon P. M. Brendel ¹, Silvan N. Bernal ¹, Cordin Arpagaus ¹, Dennis Roskosch ², André Bardow ² and Stefan S. Bertsch ^{1,*}

¹ Institute for Energy Systems, Eastern Switzerland University of Applied Sciences, 9471 Buchs, Switzerland; leon.brendel@ost.ch (L.P.M.B.); cordin.arpagaus@ost.ch (C.A.)

² Energy and Process Systems Engineering, ETH Zürich, 8092 Zürich, Switzerland; droskosch@ethz.ch (D.R.); abardow@ethz.ch (A.B.)

* Correspondence: stefan.bertsch@ost.ch

Abstract: Several theoretical studies have predicted that refrigerant mixtures with glides of more than 20 K can yield COP improvements in heat pumps for operating conditions where the temperature difference between the heat source and heat sink is large, but experimental validations and quantifications are scarce. The application of high-glide mixtures (>20 K) in industrial heat pumps in the field is, therefore, still hampered by concerns about the behavior and handling of the mixtures. This study experimentally investigates hydrocarbon (HC) mixtures R-290/600 (propane/butane) and R-290/601 (propane/pentane) and compares them to previously tested mixtures of synthetic refrigerants. Comprehensive evaluations are presented regarding COP, compressor performance, pressure drop, heat transfer, and the possibility of inline composition determination. The mixtures were tested over a range of compositions at a source inlet temperature of 60 °C and a sink outlet temperature of 100 °C, with the heat sink and heat source temperature differences controlled to 35 K. R-290/601 at a mass composition of 70%/30% was found as the best mixture with a COP improvement of 19% over R-600 as the best pure fluid. The overall isentropic compressor efficiency was similar for HC and synthetic refrigerants, given equal suction and discharge pressures. Pressure drops in heat exchangers and connecting lines were equal for synthetic and HC mixtures at equal mass flow rates. This allows higher heating capacities of HC mixtures at a given pressure drop (mass flow rate) due to their wider vapor dome. A previously developed evaporator heat transfer correlation for synthetic refrigerant mixtures was applicable to the HC mixtures. A condenser heat transfer correlation previously fitted for synthetic refrigerants performed significantly worse for HC mixtures. Composition determination during operation and without sampling was possible with a deviation of at most 0.05 mass fraction using simple temperature and pressure measurements and REFPROP for thermodynamic property calculations. Overall, high-glide HC mixtures, just like mixtures of synthetic refrigerants, showed significant COP improvements for specific operating conditions despite a decreased heat transfer coefficient. Potential problems like composition shift or poor compressor performance were not encountered. As a next step, testing high-glide mixtures in pilot-plant installations is recommended.

Keywords: glide matching; high-temperature heat pumps; hydrocarbon refrigerants; refrigerant mixtures



Citation: Brendel, L.P.M.; Bernal, S.N.; Arpagaus, C.; Roskosch, D.; Bardow, A.; Bertsch, S.S. Experimental Performance Comparison of High-Glide Hydrocarbon and Synthetic Refrigerant Mixtures in a High-Temperature Heat Pump. *Energies* **2024**, *17*, 1981. <https://doi.org/10.3390/en17081981>

Academic Editors: Fabio Polonara, Vítor António Ferreira da Costa, Sandro Nizetic and Alice Mugnini

Received: 8 March 2024

Revised: 2 April 2024

Accepted: 9 April 2024

Published: 22 April 2024



Copyright: © 2024 by the authors. Licensee MDPI, Basel, Switzerland. This article is an open access article distributed under the terms and conditions of the Creative Commons Attribution (CC BY) license (<https://creativecommons.org/licenses/by/4.0/>).

1. Introduction

“In recent years, considerable worldwide interest in heat pumps with non-azeotropic mixtures has resulted in numerous publications in which experimentally and theoretically obtained results have been discussed and compared”. This sentence, although not wrong stated today, was already written in 1987 by McLinden and Radermacher [1]. Binary and ternary mixtures

have since found a stable place among commercially used refrigerants. Soon, the R-4XX series of refrigerant names will contain 100 mixtures and require an amendment to the refrigerant nomenclature. Zeotropic (or non-azeotropic) refrigerant mixtures change temperature during an isobaric evaporation or condensation process. The temperature difference between saturated vapor and saturated liquid at some pressure is called the temperature glide. The glide of zeotropic mixtures is sometimes viewed as a benefit, but at least equally often, it is condemned because it reduces the heat transfer coefficient, as described in numerous studies ([2–8]). Most commercial refrigerant blends were designed to replace a pure fluid, so the mixture components and compositions were chosen to result in a small glide. However, along with the increasing interest in industrial heat pumps of the last few years, refrigerant mixtures with a high glide (>20 K) by design have received markedly more attention. The reason can be understood qualitatively by comparing three cycles, as sketched in Figure 1. An industrial process is hypothesized in which the return temperature comes to the condenser at 80 °C and must be heated up to 120 °C. A heat source with a large capacitance rate is available at 60 °C. As shown in Figure 1a, a subcritical butane cycle with a condensation temperature of 125 °C could bring the heat sink to 120 °C (approximate heat sink and heat source temperatures drawn with dashed lines in red and blue). However, most condensation would occur at an unnecessarily high temperature, indicating a potential for cycle improvement. Figure 1b shows a transcritical propane (R-290) cycle, where the heat rejection in the gas cooler yields a refrigerant temperature decrease matching the heat sink temperature increase well. Moreover, the high suction pressure moves the suction state of the refrigerant to an area of steeper isentropes (in a P-h diagram) and reduces the pressure ratio, both reducing the power draw of the compressor.

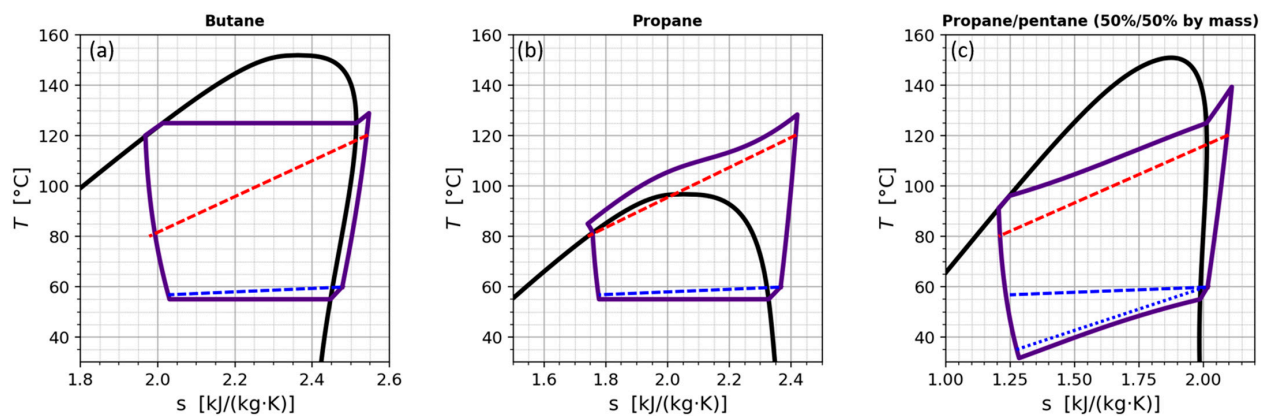


Figure 1. Comparison of vapor compression cycles: (a) Pure fluid/subcritical. (b) Pure fluid/transcritical. (c) High-glide mixture/subcritical. Dashed and dotted lines refer to the temperature change of the heat sink (red) and source (blue).

In another industrial process, the capacitance rate of the heat source might be low such that the temperature changes significantly in the evaporator. For the pure fluids, the evaporation temperature would have to drop to achieve this, resulting in a lower suction pressure, smaller volumetric heating capacity, and a higher pressure ratio.

A high-glide refrigerant mixture, as shown in Figure 1c, can supply the lower heat source outlet temperature without any change because of the temperature glide during evaporation (dotted line in Figure 1c). Hence, refrigerant mixtures with glide by design should be considered for applications where both the heat sink and heat source undergo large temperature changes (≈ 15 K or more). Brendel et al. [9] also showed experimentally that such mixtures are more robust in their performance against changing operating conditions. A widespread concern is a composition shift of high-glide mixtures due to the large difference in the normal boiling points. Both aspects are addressed in this study.

While in [9], COP improvements have been shown experimentally using mixtures of HFO/HCFO and HFC refrigerants, this study adds experimental data for hydrocarbon

(HC) refrigerants. HC refrigerants have good thermodynamic properties and are molecules occurring naturally in substantial amounts (other than synthetic refrigerants). Their environmental impact is therefore better understood, in contrast to the degradation products and TFA formation associated with many HFO and HCFO refrigerants. Finally, the range of available HC refrigerants is advantageous for mixture design over inorganic refrigerants like CO₂, water, and ammonia. Granryd [10] provided an extensive overview of the hydrocarbon family. Not only are ethane, propane, butane, pentane, and hexane available, but all have an associated alkene (ethene, propene, ...). Additionally, there are isomers and even cyclic alkanes and alkenes, further enlarging the hydrocarbon family of interest for refrigeration. The large family of molecules makes a suitable pool to draw from when designing refrigerant mixtures. A number of researchers have conducted experimental analyses of HC mixtures ([11–17]). Most of the studies focused on refrigerant mixtures with glides of less than 20 K, as listed in Brendel et al. [9]. An exception is Luo et al. ([18,19]), who showed theoretical and experimental results for mixtures of HCs with CO₂ and tested some mixtures with a glide of more than 65 K for residential cold-climate heat pumps. Their work proposes composition changes using a reservoir to adapt the mixture composition in accordance with the operating conditions.

For industrial high-temperature heat pumps, experimental work with hydrocarbon high-glide mixtures is still very scarce. More confidence is needed for the deployment of such mixtures in the field. This is highlighted by several informal discussions with industrial heat pump suppliers and designers, who request more experimental validations for the deployment of high-glide mixtures in projects with their clients. This paper addresses the literature gap by comparing experimental system-level and component-level results from HC mixtures to previously collected results from HFO, HCFO, and HFC mixtures. The comparisons focus on COP, compressor performance, pressure drop, heat transfer, and composition determination.

2. Modelling Results

A modeling example is provided in Figure 2, which was used for the mixture selection and the preparation of the test matrix. It also extends the introduction with a quantitative comparison. An industrial heat pump is assumed to have a heat sink outlet temperature of 100 °C, a source inlet temperature of 60 °C, and capacitance rates such that the temperature changes by 35 K for both the heat sink and source. An evaporator outlet superheat and subcooling at the condenser of 5 K each are assumed. The evaporator approach temperature difference (ATD) is set to 2 K, and the condenser ATD is set to 5 K (Appendix A.8 describes the definition of the ATD in more detail). An internal heat exchanger between the liquid and suction line with an effectiveness of 0.5 is used. The leveraged model is described in [20] and uses a pressure-dependent compressor efficiency correlation from [21].

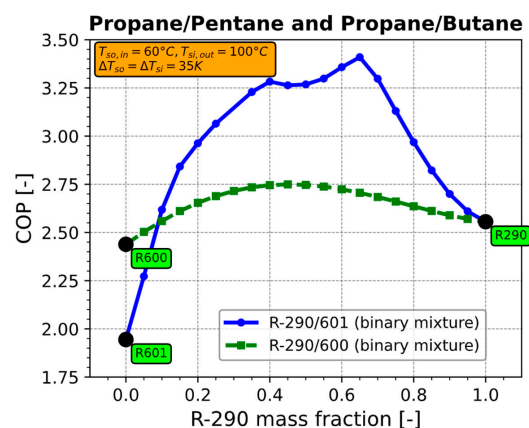


Figure 2. Modeled COP for mixtures of propane with butane and pentane as a function of the propane mass fraction.

Figure 2 shows modeling results for a propane/butane (R-290/600) and a propane/pentane (R-290/601) mixture as a function of the propane (R-290) mass fraction. The COP is graphed as a function of the propane mass fraction. The pure fluids achieve COPs between 2.56 for propane and 1.94 for pentane. Mixtures of refrigerants achieve a higher COP due to glide-matching, better compressor efficiencies, and more suitable vapor dome shapes. The COP peak occurs at 3.41 for a mixture of 65% propane by mass and 35% pentane. Propane and butane are thermodynamically more similar than propane and pentane. Therefore, mixtures result in smaller glides (maximum glide of 12 K at a propane mass fraction of 44%), insufficient for full glide matching with the heat sink and source, changing temperature by 35 K. The propane/pentane mixture has a glide of up to 44 K (at 35% propane mass fraction) such that the COP curve as a function of the mass fraction has a higher and wider dome than the propane/butane mixture (glide calculation is explained in Appendix A.1). The dent in the propane/pentane curve between a mass fraction of 40% and 65% is mainly due to an increased value of the isentropic exponent κ for those mass fractions.

3. Experimental Setup

3.1. High-Temperature Heat Pump and Water Circuit Setup

The heat pump was originally built in 2018 [22]. It was slightly modified to its current configuration in 2022, shown schematically in Figure 3. The main components of the heat pump are flat-plate heat exchangers, such as the evaporator, condenser, and internal heat exchanger, a reciprocating compressor, and an electronic expansion valve. A three-way valve guides the flow through the internal heat exchanger or bypasses it on the liquid side. Other components are an accumulator in the suction line, an oil separator downstream of the compressor, a receiver downstream of the condenser, and a filter-drier upstream of the expansion valve. The refrigerant pressure is measured at six locations throughout the cycle, and thermocouples are installed at the inlet and outlet of almost every component. Other major sensors are a Coriolis-type mass flow meter with an integrated density meter and a speed of sound sensor installed in the liquid line upstream of the expansion valve.

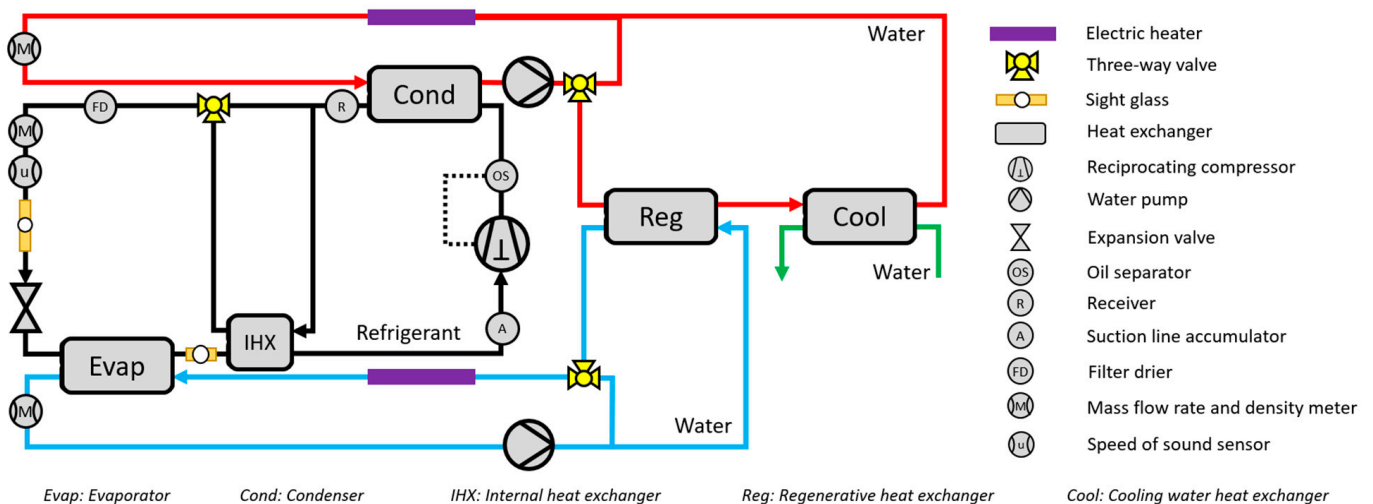


Figure 3. Schematic of the lab-scale high-temperature heat pump and secondary water circuits.

The heat pump has a heating capacity of approximately 10 kW, depending on the refrigerant and operating conditions, up to 15 kW. The compressor is inverter-driven. Compressor A was swapped out in July 2023 after dataset 1 had been collected. The following datasets, 2 and 3, were collected with Compressor B. Both compressors were of reciprocating type, had two cylinders, a total swept volume of approximately 0.15 L, and a similar shape and surface area. Both were operated with 50 Hz for most of the tested points. The following oil was employed for all tests with synthetic refrigerants:

- Name: Reniso Triton SE 170

- Type: Polyolester (POE)
- Density at 15 °C: 972 kg/m³
- Kinematic viscosity at 40 °C: 173 mm²/s
- Kinematic viscosity at 100 °C: 17.1 mm²/s
- Pourpoint: −27 °C
- Flashpoint: 260 °C
- Reference: [23]

HC tests were conducted with the following oil:

- Name: Reniso LPG 150
- Type: Polyalkylene glycol (PAG)
- Density at 15 °C: 994 kg/m³
- Kinematic viscosity at 40 °C: 149.9 mm²/s
- Kinematic viscosity at 100 °C: 26.2 mm²/s
- Pourpoint: −42 °C
- Flashpoint: 238 °C
- Reference: [24]

For the safety of experiments with hydrocarbon refrigerants, a dedicated testing container was installed, which is described in Appendix A.2.

3.2. Datasets

Three datasets are distinguished in this paper, defined by the compressor used and the refrigerant type.

1. Compressor A is used with synthetic refrigerants and mixtures (HFO, HCFO, and HFC).
2. Compressor B is used with synthetic refrigerants and mixtures (HFO, HCFO, and HFC).
3. Compressor B is used with hydrocarbon refrigerants and mixtures.

Findings from dataset 1 regarding the COP and the possibility for composition determination were published in [9,25]. Table A2 shows the exact composition of each tested mixture, the number of data points, and the range of tested pressures. Findings from dataset 2 were published in [26]. The specific tested mixtures are shown in Table A3. This study focuses on dataset 3, which has not yet been published. The data is directly compared with data from datasets 1 and 2. Specific tested mixtures of dataset 3 are listed in Table A4.

3.3. Measurement Accuracy and Steady-State Criterion

All types of sensors used are listed in Table 1 with their rated uncertainty. Cross comparison of thermocouples and pressure transducers showed agreement to a much smaller range than the rated uncertainty.

Table 1. Measurement uncertainty for used sensors. Table from [25].

Property	Measurement Principle	Uncertainty
Temperature	K-type Thermocouples	+/−1.5 K absolute
High pressure	Piezoelectric	75 kPa absolute
Low pressure	Piezoelectric	15 kPa absolute
Density	Coriolis sensor	10 kg/m ³
Mass flow rate (refrigerant)		<0.5% of reading
Mass flow rate (heat sink)		<0.5% of reading
Sound velocity	Measures time for propagation of wave between geometrically fixed speaker and receiver.	0.01 m/s absolute

The presented data points were collected at a steady state. The steady-state criterion was defined as shown in Table 2. The low side pressure was allowed to change by up to 5 kPa over the 10-min time window. To evaluate the criterion, the average of the first and the average of the last minute of a 10-min period were compared. On average, the measured changes were much less (0.5, 1.0, and 1.5 kPa for datasets 1, 2, and 3). Additional steady-state indicators were the high-side pressure, the subcooling at the expansion valve inlet, and the COP. Their maximum allowed change and average change are also shown in Table 2.

Table 2. Maximum allowed and average measured changes over 10 min for steady-state determination (calculated by comparing the average of the first and last minute).

Measurement	Max. Allowed Change over 10 min	Average Measured Change over 10 min		
		Dataset 1	Dataset 2	Dataset 3
Low side pressure	5 kPa	0.5	1.0	1.5
High side pressure	15 kPa	1.6	2.6	4.8
Subcooling at expansion valve inlet	1.5 K	0.1	0.1	0.1
COP	2.5%	0.4	4	0.5

3.4. Mixture Charging Procedure and Thermophysical Properties of Refrigerants

All refrigerants that were used to create mixtures or tested as pure refrigerants are shown in Table 3 with their critical pressure, critical temperature, normal boiling point, and heat of evaporation at a saturation temperature of 60 °C. The reference equation of state used in REFPROP is cited in the last column of the table. Thermophysical properties of mixtures were calculated with the default interaction coefficients in REFPROP.

Table 3. Thermophysical properties of refrigerants that were used as mixture components.

Refrigerant	Type	P_{crit} [kPa]	T_{crit} [°C]	T_{NBP} [°C]	$\Delta h_{fg,60^\circ C}$ [kJ/kg]	Reference for Thermodynamic Properties
R-290 (Propane)	HC	4251	97	−42	259	[27]
R-600 (n-Butane)	HC	3796	152	−1	321	[28]
R-601 (n-Pentane)	HC	3368	197	36	337	[29]
R-32	HFC	5782	78	−51	175	[30]
R-134a	HFC	4059	101	−26	155	[31]
R-1234yf	HFO	3382	95	−30	110	[32]
R-1224yd(Z)	HCFO	3337	156	14	145	[33]
R-1233zd(E)	HCFO	3624	167	18	171	[34]
R-1336mzz(Z)	HFO	2903	171	33	151	[35]

Mixtures were created by charging refrigerants one after another and tracking the charged mass of refrigerants using a scale. Mixtures were usually created exclusively by adding refrigerant. Only in the creation of mixture BC from BB and mixture BD from BC was refrigerant removed from the system (compare letters with Table A4 to find details of mixtures). The refrigerant charge was removed from the discharge line during the heat pump's operation.

In this study, the “charged mass fraction” is the mass fraction calculated from any charge additions or removals.

Refrigerants were obtained from various suppliers and had a purity of at least 99.5%.

4. Results

4.1. COP

The COP was compared for varying mixture compositions at equal operating conditions. The heat source inlet temperature was 60 °C, and the outlet temperature was 25 °C, the heat sink inlet temperature was 65 °C, and the outlet temperature was 100 °C. The evaporator outlet superheat was controlled to 5 K (upstream of the IHX), and the compressor frequency was set to 50 Hz. All refrigerant flowed through the internal heat exchanger (none was bypassed).

Figure 4 shows COP results for HC mixtures and the best-performing HFO mixture from prior work under these operating conditions. The x -axis shows the propane mass fraction for the HC mixtures and the R-1234yf mass fraction for the HFO mixture. The compressor was different for the HC tests than the HFO tests, as indicated in the legend. Still, their swept volume and overall isentropic efficiency as a function of suction and discharge pressure were very similar. Annotations show the heating capacity in kW measured on the refrigerant side for selected data points.

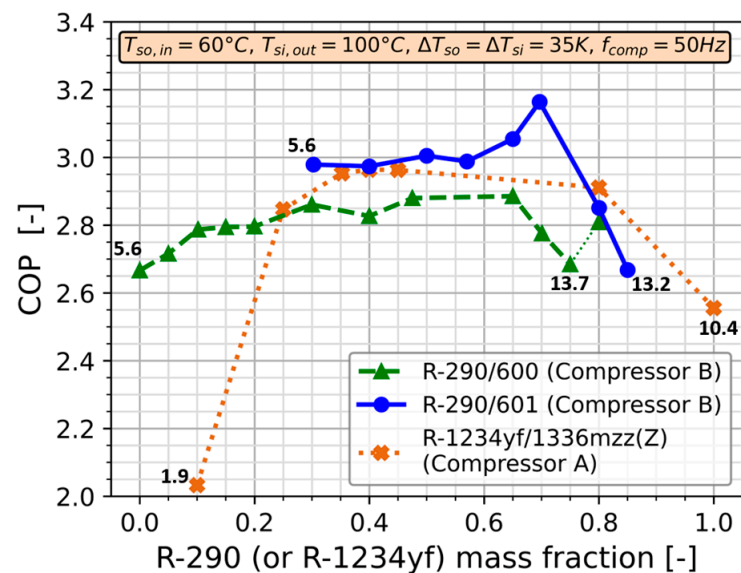


Figure 4. COP measurements from two hydrocarbon mixtures in blue and green. The best performing synthetic mixture from [9] is shown in brown, although measured with a different compressor. Annotations show the heating capacity in kW for all series endpoints.

The propane/pentane mixture is superior in COP at the given operating conditions over a range of mass fractions (blue line). For propane mass fractions from 0.3 to 0.6, the COP is close to 3. Then, the COP rises sharply to 3.16 and falls steeply as the propane mass fraction increases. The resulting horn shape of the curve is like the shape of the corresponding modeling results in Figure 2. The reason for the horn lies in the overall isentropic efficiency η_{ois} and the ratio of enthalpy differences $\Delta h_c / \Delta h_{2s}$, the product of which is the COP (additional information is provided in the Appendix A.3). Figure 5 shows how η_{ois} increases with the propane mass fraction because the suction pressure rises and the pressure ratio falls in the mass fraction range of 0.3 to 0.7 (compare with [21]). As the propane mass fraction increases, the suction pressure increases, but its positive effect on the efficiency fades. Moreover, the pressure ratio reaches an inflection point and rises again so that the overall isentropic efficiency falls. The ratio $\Delta h_c / \Delta h_{2s}$, which indicates how benign of a shape the vapor dome of the mixture has, shows a decreasing trend with an increase of the propane mass fraction because the condensation takes place closer to the critical point with less enthalpy of condensation available for heating. It decreases more steeply from a mass fraction of 0.7. The combined effect of η_{ois} and $\Delta h_c / \Delta h_{2s}$ yields the “horn shape” of the COP curve. Relationships like this are important to understand when optimizing

refrigerant mixtures, and experimental studies require a high resolution of tested mass fractions to show all trends. Possibly, the HFO series has a similar horn, which cannot be seen due to the lack of data points in the R-1234yf mass fraction range from 0.45 to 0.8 (albeit the model does not indicate such a horn).

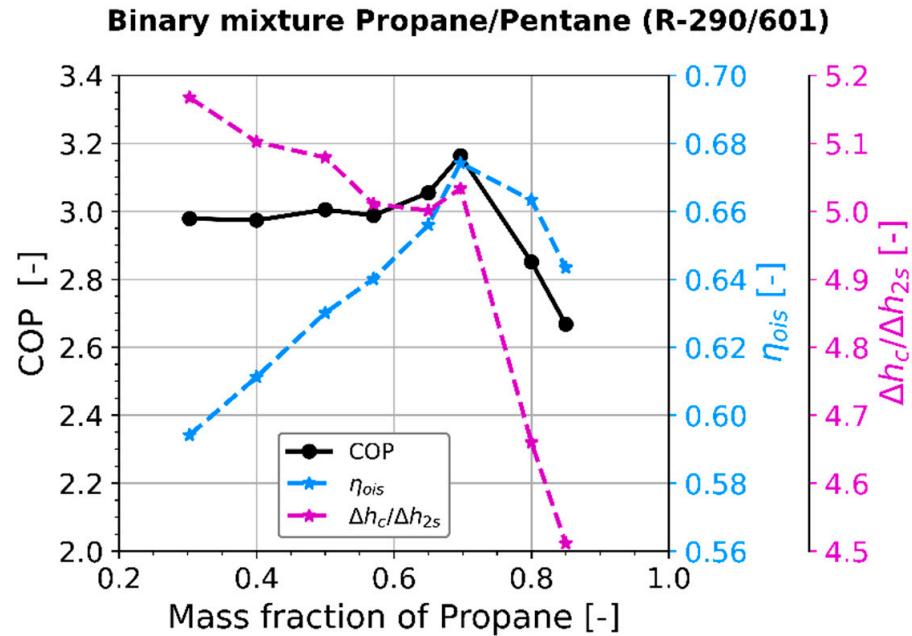


Figure 5. COP, overall isentropic compressor efficiency, and $\Delta h_c/\Delta h_{2s}$ from measurements for R-290/601 mixture as a function of the propane mass fraction.

The propane/butane mixture reaches a maximum glide of 12 K at a dew point temperature of 60 °C, much less than the glide of propane/pentane, which reaches 43.5 K at the maximum. The COP shown in Figure 4 changes, therefore, less quickly as a function of the mass fraction. The series reaches a COP maximum at a mass fraction of approximately 0.5, as predicted in the initial modeling example (Figure 2). The series has one significant outlier, which is shown but connected only with a dotted line. The higher COP is due to smaller condenser heat losses at this point (5% as opposed to 8 to 10% for the other data points).

Pure R-600 resulted in a COP of 2.67, which is higher than the COP of pure HFO and HCFO refrigerants as presented in [9] ($COP_{R1234yf} = 2.55$, $COP_{R1224yd(Z)} = 2.32$, $COP_{R1233zd(E)} = 2.24$). Pure R-290, R601, and R-1336mzz(Z) could not be measured since their pressures at the operating conditions would be too high or too low to be assessed on the setup. Pure R-601 and R-1336mzz(Z) are expected to have extremely low COPs on this system due to their low suction pressure and, therefore, low compressor efficiency.

4.2. Compressor Performance

The performance of compressor A with synthetic refrigerants and their mixtures was thoroughly discussed in [21]. Correlations for the overall isentropic and volumetric efficiency were fitted as follows for dataset 1:

$$\eta_{vol} = \frac{\dot{m}}{\rho_1 V_{swept} f} = 1 - b_0 \cdot (P_r - 1)^{b_1} \quad (1)$$

$$\eta_{ois} = \frac{\dot{m}(h_{2s} - h_1)}{\dot{W}} = a_0 - \frac{0.6}{(P_r - a_1)^{a_2} \cdot P_s} - a_3 \cdot P_r^{1.8} \quad (2)$$

In these equations, \dot{m} is the refrigerant mass flow rate, ρ_1 the suction density, V_{swept} the swept volume of the compressor, f the compressor frequency, h_1 the suction enthalpy,

h_{2s} the enthalpy after an isentropic compression to the discharge pressure, \dot{W} the electrical power draw of the compressor, η_{vol} the volumetric efficiency, η_{ois} the overall isentropic efficiency, P_r the pressure ratio and P_s the suction pressure. a_i and b_i are coefficients, as shown in Table 4. For the 258 data points in dataset 1, the isentropic efficiency was predicted on average with an error of 0.018 (Table 5). The maximum error was 0.049. Applying the correlation with the original coefficients (Table 4) to dataset 2 showed an average deviation of 0.01 and a maximum deviation of 0.027. It can, therefore, be inferred that compressors A and B are very comparable in terms of the overall isentropic efficiency. Furthermore, when applying the correlation to the HC refrigerants in dataset 3, the maximum deviation increased to 0.103, but the average deviation was still only 0.024. Overall, since the correlation applies to all three datasets, it can be inferred for the tested compressors that the isentropic compressor efficiency is mostly a function of the suction and discharge pressure and that effects of the different refrigerants are small as long as compared to the basis of pressures. The same reasoning and conclusion hold for the volumetric efficiency. An improved correlation capturing the effects of hydrocarbons on the isentropic efficiency, as well as a correlation for the heat losses, is beyond the scope of this paper but published in [36].

Table 4. Coefficients for empirical descriptions of compressor efficiency.

Coefficient	b_0 [-]	b_1 [-]	a_0 [-]	a_1 [-]	a_2 [1/kPa]	a_3 [-]
Value	0.08244	0.72773	0.66981	0.01466	0.00838	0.00102

Table 5. Performance of correlations from [21] for all three datasets.

	Dataset 1 (Compressor A, Synthetic Refrigerants)	Dataset 2 (Compressor B, Synthetic Refrigerants)	Dataset 3 (Compressor B HC Refrigerants)
Number of data points	258	49	61
Overall isentropic efficiency	Avg. dev.: 0.018 Max. dev.: 0.049	Avg. dev.: 0.010 Max. dev.: 0.027	Avg. dev.: 0.024 Max. dev.: 0.103
Volumetric efficiency	Avg. dev.: 0.023 Max. dev.: 0.064	Avg. dev.: 0.012 Max. dev.: 0.031	Avg. dev.: 0.027 Max. dev.: 0.079

4.3. Pressure Drop

Pressure drop occurs in the pipes and heat exchangers throughout the system. Although it does usually not strongly affect the COP, it should be considered in the system design and modeling. Especially with the internal heat exchanger, the suction line pressure drop (evaporator outlet to compressor inlet) was vital to improve the model performance.

Figure 6 shows the suction line pressure drop of all data points with pure fluids or mixtures consisting of HFO, HCFO, and HFC refrigerants in black dots. Pure fluids or mixtures from the HC family are indicated with red crosses. All data shown was taken at a compressor frequency of 50 Hz. The pressure drop is a linear function of the mass flow rate, the expected result predicted from single-phase pressure drop equations (derived in Appendix A.4). When plotted as a function of the mass flow rate \dot{m} , as in Figure 6 (left), the pressure drops of synthetic and HC refrigerants show linear trends with equal slopes. However, since the vapor domes of HC are typically wider in the P-h diagram than the domes of HFO refrigerants (compare with Figure 7), HC refrigerants achieve a higher heating capacity at a given mass flow rate. This effect is shown in Figure 6 (right), where the pressure drop is plotted as a function of the refrigerant side heating capacity \dot{Q}_{cond} . In this representation, the HC refrigerant pressure drop is approximately half of the synthetic refrigerant pressure drop at any given heating capacity. The pressure drops in the evaporator and condenser show similar trends, albeit with more scatter due to the

manifold inlet and outlet conditions and the combination of single- and two-phase flow in the heat exchangers.

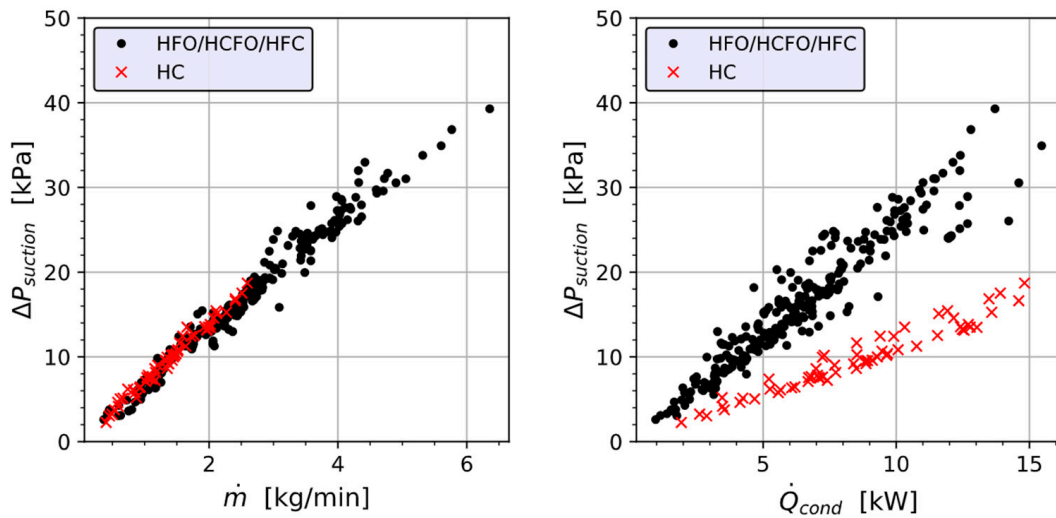


Figure 6. Pressure drop in the suction line as a function of mass flow rate and heating capacity.

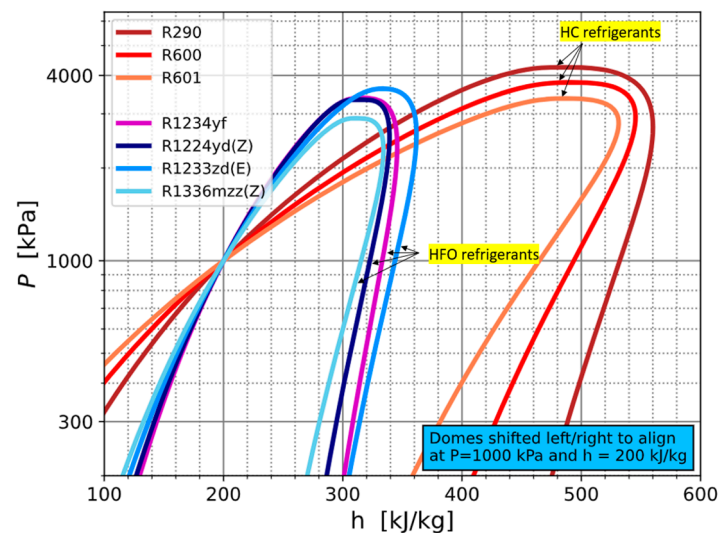


Figure 7. Comparison of vapor domes of HC and HFO refrigerants in P-h diagram.

4.4. Heat Transfer

4.4.1. Introduction to Correlations

Early test results presented in [20] using refrigerant mixtures with a glide of up to 17 K at a dew point temperature of 60 °C showed evaporator approach temperature differences (ATD) of 10 K in some operating conditions (definition and explanation of the measurement of the ATD is provided in Appendix A.8). At the same operating conditions, other mixtures or pure fluids had an evaporator ATD of only 1 K. While part of this large discrepancy was attributable to an increased absolute heat transfer rate, this was insufficient to explain the different approach temperatures measured. Predicting approach temperature differences well was important to obtain an overall system model with strong prediction capabilities. Therefore, Brendel et al. proposed heat transfer correlations for the evaporator and condenser in [37]. Those were fitted and evaluated for dataset 1. Available heat transfer correlations from the open literature were not applicable because of the glides of the mixtures and because the ranges of operating conditions within the dataset were unusually wide. The following particularities should be mentioned:

- The correlations are based on more than 250 data points from four different pure fluids and 25 binary or ternary mixtures thereof with temperature glides of up to 42 K.
- The operating conditions covered are very wide. For example, the evaporator outlet superheat ranged from 1.9 to 33.9 K and the evaporator inlet quality of the refrigerant ranged from 0.14 to 0.77. The heat transfer rate ranged from 0.3 to 9.8 kW, and the refrigerant inlet temperature ranged from -15 to 73 °C.
- The correlations were designed using a case structure. For the evaporator and condenser, criteria for a data group were found where the ATD was below 1.5 K. The correlations predict an ATD of 1 K for all the data points meeting the criteria. Only the rest of the data is correlated with physically meaningful and specially fitted coefficients.
- The correlations are based on a lumped approach to simplify their application (as opposed to a moving boundary or finite element method).

The shortcomings of the two correlations are as follows:

- The correlations are dimensional and fitted only to one evaporator and one condenser. Unlike correlations for the heat transfer coefficient only, the presented correlations cannot be used confidently for other heat exchangers.
- The evaporator was oversized for some operating conditions, which may have caused a laminar flow on the water side. Additionally, refrigerant maldistribution was detected for some operating conditions by comparing two temperature readings downstream of the evaporator at different distances.

Tables 6–8 summarize the ranges of experimental data and the performance of the correlations for datasets 1, 2, and 3. At the top of the table, the pure refrigerants and the tested mixtures are presented. A list of letters allows cross-referencing of mixtures with Tables A2–A4 (one letter represents a mixture unique in components and composition). The table also shows ranges of operating conditions for certain variables relevant to heat transfer in plate heat exchangers. The last section shows the performance of the correlation. The correlation was applied to each data point using the appropriate input measurements. For the evaporator correlation, the performance indicator is the prediction of the evaporator inlet temperature. For example, in dataset 1, for 73% of the data, the evaporator inlet temperature was predicted within ± 3 K, and for another 25% within ± 6 K (compare with area in table highlighted in green). Only 2% of the data was predicted with a deviation greater than ± 6 K. For the condenser correlation, the indicator for performance is the saturated liquid temperature of the refrigerant. For 85% of all data points, this was predicted to be within ± 3 K.

It could be argued that a deviation of ± 3 K is exceedingly high. However, with the application being system-level modeling and the wide ranges of operating conditions and mixture properties, ± 3 K was considered a legitimate goal for this correlation and used as the main indicator.

In the following, the two correlations are presented. Then, dataset 2 is used to validate the correlation for HFO/HCFO and HFC refrigerants and mixtures, and dataset 3 is used to evaluate the correlations for HC refrigerants. The coefficients are not changed for these comparisons.

Table 6. Description of dataset 1 and performance of correlation. The dataset was used to build the correlation. Main performance results of correlation highlighted in green.

Dataset 1 (to Build Correlation)	Evaporator	Condenser
Types	Flat plate heat exchangers in counterflow configuration	
Refrigerants and mixtures	<p><i>Pure:</i> R1336mzz(Z), R1233zd(E), R1224yd(Z), R1234yf</p> <p><i>Mixtures:</i> R1336mzz(Z)/R1234yf (6), R1233zd(E)/R1234yf (3), R1224yd(Z)/R32 (5), R1224yd(Z)/R32/R1336mzz(Z) (1), R1224yd(Z)/R32/R1234yf (8), R1336mzz(Z)/R1234yf/R32 (2) *</p> <p><i>Letters (for reference with Table A2):</i> A, B, C, D, E, F, G, H, J, K, L, M, N, O, P, Q, R, S, T, V, W, X, Y, Z, AA, AB, AC, AD, AE</p>	

Table 6. Cont.

Dataset 1 (to Build Correlation)	Evaporator			Condenser		
Conditions to include points	<ul style="list-style-type: none"> - Visually verified subcooling at the expansion valve inlet - Steady-state duration at least 8 min 			<ul style="list-style-type: none"> - Visually verified subcooling at the expansion valve inlet - Steady-state duration at least 8 min - Minimum condenser inlet superheat of 1 K 		
Number of data points	274			266		
Ranges of experimental data	Variable	Min	Max	Variable	Min	Max
	$\Delta T_{gl,60}$ [K]	0	42	$\Delta T_{gl,60}$ [K]	0	42
	$\Delta T_{sh,e,out}$ [K]	1.9	33.9	$\Delta T_{sh,c,in}$ [K]	1.3	47.1
	$x_{e,in}$ [-]	0.14	0.77	$\Delta T_{sc,c,out}$ [K] **	-6.0	8.0
	ΔT_{so} [K]	0.2	43.6	ΔT_{si} [K]	0.5	44.9
	\dot{m}_{ref} [kg/min]	0.16	6.88	\dot{m}_{ref} [kg/min]	0.27	6.88
	\dot{m}_{water} [kg/min]	0.9	28.1	\dot{m}_{water} [kg/min]	0.6	29.0
	P_{ref} [kPa]	48	984	P_{ref} [kPa]	208	3229
	\dot{Q} [kW] ***	0.3	9.8	\dot{Q} [kW] ***	0.8	14.0
	$T_{so,out}$ [°C]	4	98	$T_{si,out}$ [°C]	34	144
	$T_{ref,in}$ [°C]	-15	73	$T_{ref,in}$ [°C]	60	158
$\Delta T_{atd,e}$ [K]	-1.1	15.8	$\Delta T_{atd,c}$ [K]	-1.1	5.7	
Performance: Prediction of saturation temperature	$T_{e,in,meas} - T_{e,in,calc}$			$T_{cond,f,meas} - T_{cond,f,calc}$		
	±0 to 3 K			±0 to 3 K		
	73%			85%		
	±3 to 6 K			±3 to 6 K		
	25%			10%		
	±6 to 10 K			±6 to 10 K		
2%			3%			
±10 to 25 K			±10 to 25 K			
0%			1%			
> ±25 K or nan			> ±25 K or nan			
0%			1%			

* Numbers in parentheses show the number of different compositions tested. ** The reason for negative subcooling is not yet clear. Subcooling was confirmed visually through a sight glass. Potentially, the bubble lines of the mixtures are predicted incorrectly by REFPROP. Subcooling was visually confirmed for each data point only at the expansion valve inlet, not at the condenser outlet. *** Refrigerant-side measurement.

Table 7. Description of dataset 2 and performance of correlation. Dataset was used to verify correlation with HFO/HCFO/HFC refrigerants. Main performance results of correlation highlighted in green.

Dataset 2 (to Validate Correlation)	Evaporator			Condenser		
Types	Flat plate heat exchangers in counterflow configuration					
Refrigerants and mixtures	Pure: R-1224yd(Z), R134a Mixtures: R-1234yf/1224yd(Z) (3), R-1234yf/1224yd(Z)/1336mzz(Z) (2) * Letters (for reference with Table A3): AH, AI, AJ, AK, AM, AN					
Conditions to include points	<ul style="list-style-type: none"> - Measured subcooling of at least 0.2 both at condenser outlet and expansion valve inlet - Steady-state duration at least 8 min 			<ul style="list-style-type: none"> - Measured subcooling of at least 0.2 both at condenser outlet and expansion valve inlet - Minimum condenser inlet superheat of 0.2 K - Steady-state duration at least 8 min 		
Number of data points	66			66		
Ranges of experimental data	Variable	Min	Max	Variable	Min	Max
	$\Delta T_{gl,60}$ [K]	0.1	16	$\Delta T_{gl,60}$ [K]	0	16
	$\Delta T_{sh,e,out}$ [K]	0.1	15.8	$\Delta T_{sh,c,in}$ [K]	0.3	60.5
	$x_{e,in}$ [-]	0.15	0.60	$\Delta T_{sc,c,out}$ [K]	0.3	6.6
	ΔT_{so} [K]	2.74	25.2	ΔT_{si} [K]	4.8	25.1
	\dot{m}_{ref} [kg/min]	1.17	5.60	\dot{m}_{ref} [kg/min]	1.17	5.60

Table 7. Cont.

Dataset 2 (to Validate Correlation)	Evaporator		Condenser			
Ranges of experimental data	\dot{m}_{water} [kg/min]	1.9	30.9	\dot{m}_{water} [kg/min]	2.5	29.0
	P_{ref} [kPa]	165	806	P_{ref} [kPa]	909	2732
	\dot{Q} [kW] **	2.3	10.4	\dot{Q} [kW] **	3.0	15.5
	$T_{so,out}$ [°C]	15	67	$T_{si,out}$ [°C]	33	123
	$T_{ref,in}$ [°C]	11.8	61	$T_{ref,in}$ [°C]	69	148
	$\Delta T_{atd,e}$ [K]	−1.1	8.4	$\Delta T_{atd,c}$ [K]	−0.2	6.6
Performance: Prediction of saturation temperature	$T_{e,in,meas} - T_{e,in,calc}$		$T_{cond,f,meas} - T_{cond,f,calc}$			
	±0 to 3 K		92%	±0 to 3 K		95%
	±3 to 6 K		8%	±3 to 6 K		5%
	±6 to 10 K		0%	±6 to 10 K		0%
	±10 to 25 K		0%	±10 to 25 K		0%
	> ±25 K or nan		0%	> ±25 K or nan		0%

* Numbers in parentheses show the number of different compositions tested. ** Refrigerant-side measurement.

Table 8. Description of dataset 3 and performance of correlation. The dataset was used to assess the correlation for applicability to HC refrigerants. Main performance results of correlation highlighted in green and orange.

Dataset 3 (Check Applicability to HC)	Evaporator		Condenser			
Types	Flat plate heat exchangers in counterflow configuration					
Refrigerants and mixtures	Pure: R-600					
	Mixtures: R-290/600 (11), R-290/601 (8) *					
Conditions to include points	Letters (for reference with Table A4): AO, AP, AQ, AR, AS, AT, AU, AV, AW, AX, AY, AZ, BA, BB, BC, BD, BE, BF, BG, BH, BI					
	- Measured subcooling of at least 0.2 both at condenser outlet and expansion valve inlet	- Measured subcooling of at least 0.2 both at condenser outlet and expansion valve inlet	- Minimum condenser inlet superheat of 0.2 K	- Minimum condenser inlet superheat of 0.2 K		
	- Steady-state duration at least 8 min	- Steady-state duration at least 8 min	- Steady-state duration at least 8 min	- Steady-state duration at least 8 min		
Number of data points	62		62			
Ranges of experimental data	Variable	Min	Max	Variable	Min	Max
	$\Delta T_{gl,60}$ [K]	0	43	$\Delta T_{gl,60}$ [K]	0	43
	$\Delta T_{sh,e,out}$ [K]	0	17	$\Delta T_{sh,c,in}$ [K]	8.3	52.6
	$x_{e,in}$ [−]	0.08	0.71	$\Delta T_{sc,c,out}$ [K]	2.0	14.4
	ΔT_{so} [K]	3.7	35.2	ΔT_{si} [K]	4.8	35.6
	\dot{m}_{ref} [kg/min]	0.40	2.59	\dot{m}_{ref} [kg/min]	0.40	2.59
	\dot{m}_{water} [kg/min]	1.8	30.9	\dot{m}_{water} [kg/min]	2.08	26.1
	P_{ref} [kPa]	150	730	P_{ref} [kPa]	281	3128
	\dot{Q} [kW] **	1.1	11.9	\dot{Q} [kW] **	1.9	14.8
	$T_{so,out}$ [°C]	14	56	$T_{si,out}$ [°C]	28	124
	$T_{ref,in}$ [°C]	−4	53	$T_{ref,in}$ [°C]	61	160
	$\Delta T_{atd,e}$ [K]	−1.0	8.2	$\Delta T_{atd,c}$ [K]	0.3	10.2
Performance: Prediction of saturation temperature	$T_{e,in,meas} - T_{e,in,calc}$		$T_{cond,f,meas} - T_{cond,f,calc}$			
	± 0 to 3 K		82%	±0 to 3 K		50%
	±3 to 6 K		7%	±3 to 6 K		11%
	±6 to 10 K		11%	±6 to 10 K		7%
	±10 to 25 K		0%	±10 to 25 K		24%
	>±25 K or nan		0%	>±25 K or nan		8%

* Numbers in parentheses show the number of different compositions tested. ** Refrigerant-side measurement.

4.4.2. Evaporator Correlation

The design of the evaporator correlation was simplified by dividing the data into two groups distinguished by having an ATD of more or less than 1.5 K. For data with an ATD < 1.5 K, the assignment of 1 K as the ATD is sufficiently accurate for any system-level modeling. It was found by graphical analysis of the data that data points with a small ATD typically fulfilled the condition $\Delta T_{so}/\Delta T_{sh,e,out} < 1$, where ΔT_{so} is the temperature difference of the heat source and $\Delta T_{sh,e,out}$ is the refrigerant superheat at the evaporator outlet (compare with Figure A4 (left) in Appendix A). This condition made the occurrence of the pinch point at the refrigerant outlet and heat source inlet highly likely, allowing a small ATD. Two major dependencies were found for the remaining data when looking at an overall UA value defined based on the driving temperature difference measured from the source inlet temperature $T_{so,in}$ to the refrigerant inlet temperature $T_{e,in}$. The UA value was mainly dictated by the heat source mass flow rate and the glide of the mixture. The dependencies are shown graphically in the Appendix A in Figure A4 (right). The correlation is defined as follows:

If $\Delta T_{so}/\Delta T_{sh,e,out} > 1$: (case 1)

$$\Delta T_{drive} = T_{so,in} - T_{e,in} \quad (3)$$

$$UA_{overall,so} = \frac{\dot{Q}}{\Delta T_{drive}} \quad (4)$$

$$UA_{overall,so} = \left(1 - \exp\left(-a_0 \dot{m}_{so} \frac{a_1 + \Delta T_{gl,60}}{a_1}\right)\right) \left(1 - \frac{\Delta T_{gl,60}^{a_3}}{a_2}\right) \quad (5)$$

$$a_0 = 0.07 \left[\text{minkg}^{-1}\right], a_1 = 20 \text{ [K]}, a_2 = 13 \left[\text{K}^{0.6}\right], a_3 = 0.6 [-]$$

Else ($\Delta T_{so}/\Delta T_{sh,e,out} < 1$): (case 2)

Assign approach temperature difference of 1 K. Evaluate where the pinch point occurs iteratively!

\dot{Q} is the heat transfer rate in kW, and $\Delta T_{gl,60}$ is the glide of the mixture in K at a dewpoint temperature of 60 °C. The heat source mass flow rate \dot{m}_{so} should be plugged in with the units kg/min.

4.4.3. Condenser Correlation

The condenser correlation design was also simplified by carving out the group of data points with an ATD of less than 1.5 K. For the condenser data, two conditions were necessary to define this subset $\Delta T_{si} < 15$ K and $\Delta T_{gl,60} < 5$ K, where ΔT_{si} is the sink temperature difference and $\Delta T_{gl,60}$ is the glide of the mixture as introduced earlier. For the remaining data, it was necessary to further distinguish between data points with $\Delta T_{si} > 15$ K and data points with $\Delta T_{si} < 15$ K but $\Delta T_{gl,60} > 5$ K. The driving potential for the condenser is defined as the difference between the dew point temperature of the refrigerant $T_{cond,g}$ and the sink inlet temperature $T_{si,in}$. The complete correlation is written as follows:

If $\Delta T_{si} > 15$ K: (case 1)

$$\Delta T_{drive} = T_{cond,g} - T_{si,in} \quad (6)$$

$$UA_{overall,si} = \frac{\dot{Q}}{\Delta T_{drive}} \quad (7)$$

$$UA_{overall,si} = \dot{m}_{si} \left(b_0 - b_1 \frac{\Delta T_{gl,60}}{\Delta T_{si}}\right) \quad (8)$$

$$b_0 = 0.087 \left[\text{kWK}^{-1}\text{minkg}^{-1}\right], b_1 = 0.017 \left[\text{kWK}^{-1}\text{minkg}^{-1}\right]$$

If $\Delta T_{si} < 15$ K and $\Delta T_{gl,60} > 5$ K : (case 2)

$$UA_{overall,si} = \dot{m}_{ref} \left(c_0 - c_2 \left(\Delta T_{gl,60} - c_1 \right) \right) \quad (9)$$

$$c_0 = 0.225 \left[\text{kWK}^{-1} \text{minkg}^{-1} \right], c_1 = 5 \text{ [K]}, c_2 = 0.0031 \left[\text{kWK}^{-1} \text{minkg}^{-1} \text{K}^{-1} \right]$$

Else ($\Delta T_{si} < 15$ K and $\Delta T_{gl,60} < 5$ K): (case 3)

Assign approach temperature difference of 1 K. Evaluate where the pinch point occurs iteratively!

\dot{Q} is the heat transfer rate in the condenser in kW, \dot{m}_{si} and \dot{m}_{ref} are the mass flow rates of the heat sink and refrigerant, respectively, in kg/min. All other symbols have been introduced or are simple coefficients.

4.4.4. Interpretation of Results

The correlations fitted to dataset 1 were assessed for dataset 2, which contains data from two pure fluids, one binary mixture at three compositions, and one ternary mixture at two different compositions. Again, the evaporator inlet conditions were predicted for each datapoint and compared with the measured inlet condition. 92% of the data had a deviation of only ± 3 K, and all other data points were predicted to have a deviation of at most ± 6 K (Table 7). Similarly, the condenser correlation performed better on the validation dataset than on the original dataset. Since the validation set is smaller and because data points were not collected at the same operating conditions, dataset 1 may have more extreme data points, which are not captured as well by the correlations.

The correlation was then also applied to dataset 3 with the fluids, data ranges, and performance shown in Table 8. The evaporator correlation predicted 82% of the data points with a maximum deviation of ± 3 K. This indicates that the correlation can be used with confidence for hydrocarbons. However, 11% of the data points were predicted with an absolute deviation of 6 to 10 K. Figure 8 adds information to the comparison of synthetic and natural refrigerants. The left-hand side plot compares synthetic and HC refrigerants as a function of the heat transfer rate. It shows more HC data points beyond the ± 6 K line, making up the 11% mentioned before. Figure 8 (right) shows only HC data points and distinguishes the method used in the correlation. It shows that the outliers are caused by the first case in the correlation, while the case assigning a fixed pinch point of 1 K produced results within the ± 3 K limits. Both methods were used for high heat transfer rates, but for heat transfer rates of less than 4 kW, only the fixed ATD method was used.

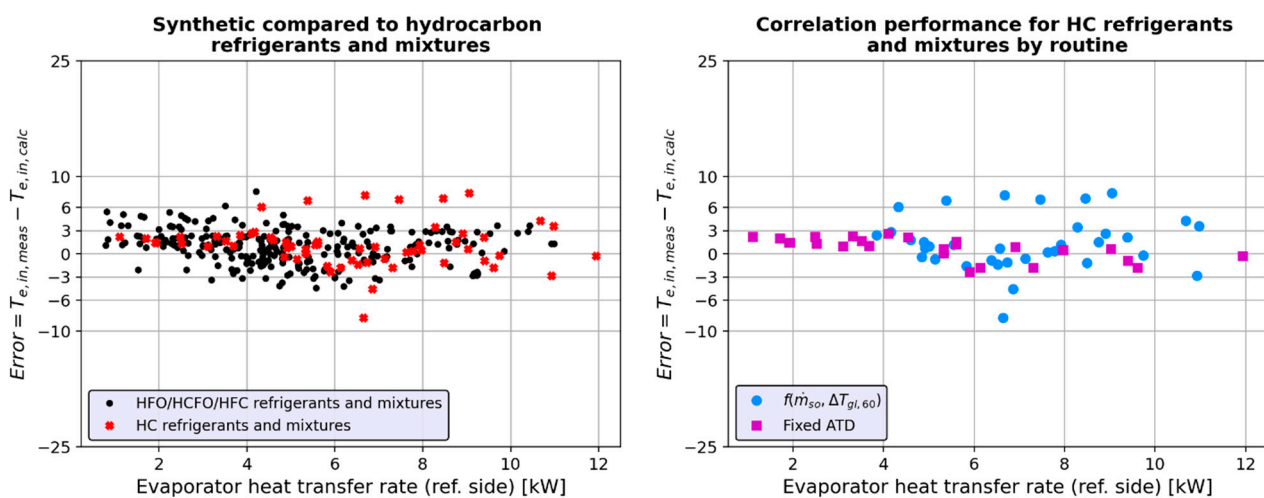


Figure 8. Performance of evaporator correlation. (Left) Comparison of HFO/HCFO/HFC data versus HC data. (Right) Comparison of methods only for the HC dataset.

In contrast to the evaporator correlation, the condenser correlation performed poorly. Only 61% of the data points were predicted with a deviation of less than ± 6 K (highlighted in Table 8 in orange). Figure 9 (right) displays the deviations distinguished by the three different cases of the correlation. Data points predicted in case 3 with a fixed ATD of 1 K had small deviations. All the data points with a deviation of more than +10 K were predicted by case 1 of the correlation. On the other hand, all the outliers with a deviation of less than -10 K were from case 2. Hence, the conditions for assigning a fixed ATD seem useful, but the rest of the correlation must be refitted to be valid for HC refrigerants and their mixtures. A new correlation is beyond the scope of this paper. However, given the positive results of the evaporator correlation and the condenser correlation for synthetic refrigerant data, it should be possible to craft a better correlation, ideally covering the data points for all types of refrigerants.

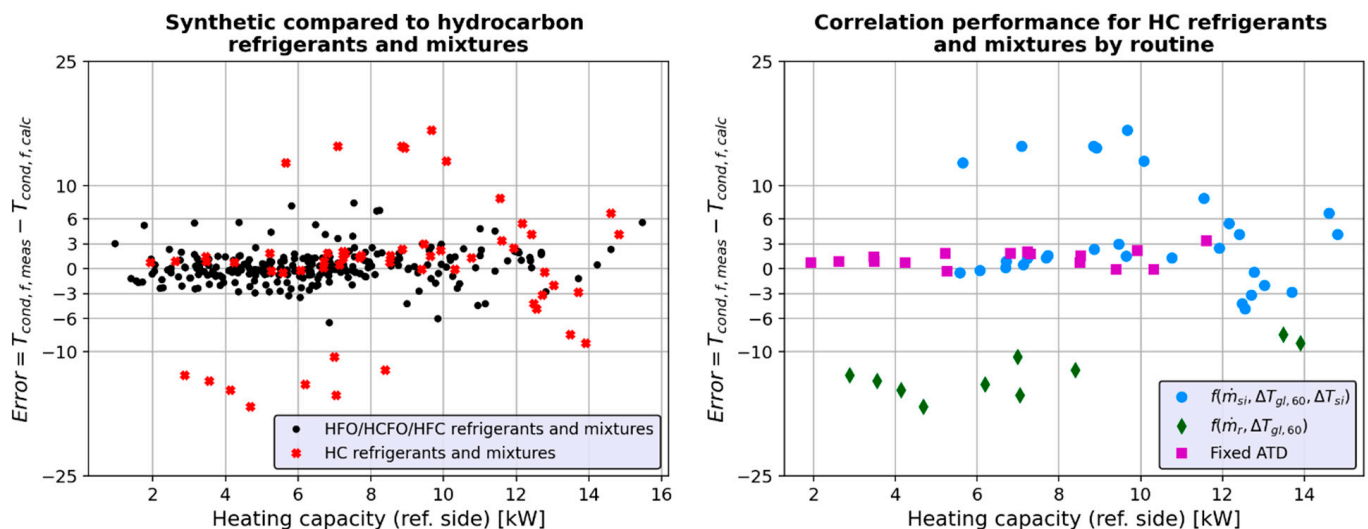


Figure 9. Performance of condenser correlation. (Left) Comparison of HFO/HCFO/HFC data versus HC data. (Right) Comparison of methods only for the HC dataset.

5. Thermophysical Properties and Composition Determination

Brendel et al. [25] compared measured and calculated data, where the calculations rely on thermophysical property predictions from REFPROP. For example, the density in the liquid line can be measured with an appropriate sensor and calculated using temperature and pressure measurements as inputs to a thermodynamic property function. If there is an agreement of measurements and calculations, this could be a coincidence. However, it is more likely that both the REFPROP mixture models and the charging and measurement procedures have a high quality and confirm each other. This method can prove a REFPROP mixture model trustworthy for system level and refrigerant mixture design. Apart from density, such comparisons can be performed on five other properties. The complete six methods introduced in [25] are listed as follows:

- Evaporator inlet temperature.
- Dewpoint temperature
- Liquid phase density
- Liquid phase speed of sound
- Condenser heat transfer rate
- Resting pressure

More information about the methods can be found in the Appendix (Appendix A.7) or the respective publication ([25]).

A comparison of measurements and calculated values for all six methods is shown for the hydrocarbon dataset in the Appendix A in Figure A3. Deviations of measurements and calculated values have the unit Kelvin for temperatures and percent for all other methods.

Overall, the deviations between measurements and calculations are small and similar in magnitude for the HC mixtures compared to differences in synthetic refrigerant mixtures as shown in [25]. It is possible to calculate the mixture composition based on the six different comparisons by solving for the mass fraction of the mixture that yields the measured value when plugged into the calculation. The iteratively obtained mass fraction can then be compared against the mass fraction as per the manual charging of the heat pump with refrigerant. The results for each data point are shown in Figure 10. One subplot is shown for each method (columns) and each tested mixture (rows). A black vertical line indicates the composition charged to the system based on weight measurements. Each marker represents one datapoint, for which the composition was calculated according to the method of the respective column. The first number in the top left-hand side corner of a subplot shows the number of data points in the plot. The percentage number next to it shows the share of data points in the subplot (100% for all subplots in Figure 10). \bar{x} shows the average of all calculated compositions for one subplot. Δx shows the deviation of \bar{x} from the charged mass fraction as indicated in Table A4. A green color was assigned to any deviation Δx smaller than 0.025. Yellow was assigned for $0.025 < \Delta x \leq 0.055$. Orange was assigned to any $\Delta x > 0.055$.

The best method for composition determination for dataset 3 is the Evaporator Inlet Temperature Method. On average, this method predicted the composition with a deviation of 0.02 and a maximum deviation of 0.05 (this was 0.02 and 0.06 for the HFO/HCFO/HFC series in dataset 1, as shown in [25]). Calculating the composition from the density resulted in an average deviation of 0.06 and a maximum deviation of 0.1, significantly worse than for the HFO/HCFO/HFC data set (0.01 and 0.03). The speed of sound method performed similarly for both datasets, with an average deviation of 0.04 and a maximum of 0.08 for the HC dataset (0.03 and 0.06 for the HFO/HCFO/HFC dataset). The energy balance method performed poorly, just like for the HFO/HCFO/HFC data. This is easily explained by the heat losses, which enforce a mismatch between the refrigerant and water side heat transfer rates and undermine any attempt for composition determination. The dewpoint temperature and resting pressure methods did not have enough data points for a proper evaluation. These methods are expected to work as well as they had for the HFO/HCFO/HFC dataset. However, neither method is very practical. The Dewpoint Method requires saturated evaporator outlet conditions, which must be visually confirmed through a sight glass. The Resting Pressure method requires the system to have complete mechanical and thermal equilibrium.

Analyzing the reasons for the worsened performance of the density method is beyond the scope of this paper. Future work will evaluate the methods with higher accuracy sensors and a more in-depth analysis of the thermophysical properties as a function of mass fractions for different refrigerants. Overall, the results show that composition determination during operation works well and does not require sampling of the refrigerant mixture.

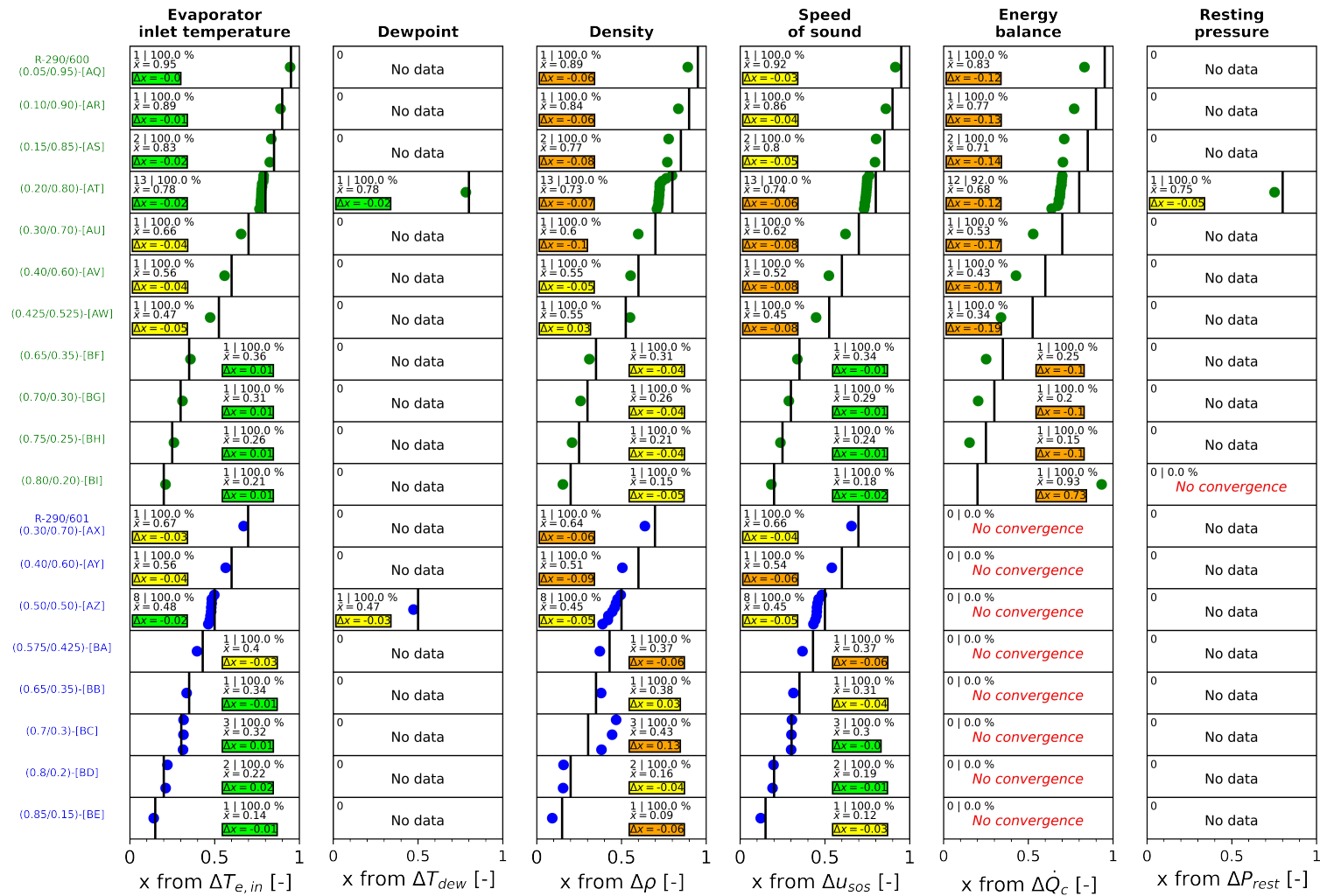


Figure 10. Composition determination is based on six different methods. For each subplot, the top left number is the number of data points shown in the plot. Percentage value: The number of data points shown in the percentage of available data points (less than 100% if the method fails to converge for any data points). \bar{x} : Average composition of all data points. Number in colored box: Deviation of average calculated mass fraction from charged mass fraction.

6. Conclusions

Propane/butane (R-290/600) and propane/pentane (R-290/601) mixtures were experimentally evaluated at various compositions in a laboratory-scale high-temperature heat pump. The results are compared with a large body of HFO/HCFO/HFC data from prior work.

For the operating point with a sink inlet and outlet temperature of 65 °C and 100 °C and a source inlet and outlet temperature of 60 °C and 25 °C, the propane/pentane mixture with a propane mass fraction of 70% achieved a COP of 3.16, which was 19% higher than the COP from the best pure fluid (butane).

The overall isentropic and volumetric compressor efficiency was similar for the HC data and the HFO/HCFO/HFC when compared based on suction and discharge pressure. A correlation was presented, which predicts the efficiencies with an average deviation of less than 0.03. The pressure drop at a given mass flow rate was comparable for data points from all refrigerants. Therefore, for any given heating capacity, HC refrigerants have approximately half the pressure drop of synthetic refrigerants due to their significantly wider vapor dome.

An evaporator heat exchanger correlation accounting for temperature glide, originally fitted for synthetic refrigerants, performed well for HC refrigerant mixtures, too. A condenser correlation performed significantly worse for HC refrigerant mixtures than for synthetic refrigerants and must be restructured. Both correlations should be improved to be dimensionless.

Good alignment was found between various thermodynamic property measurements and predictions from REFPROP for all mixtures. Inline composition determination was demonstrated with different methods. The Evaporator Inlet Temperature method performed best with an average prediction of the mass fraction within 0.02 from the charged mass fraction.

Overall, high-glide mixtures showed significant COP improvements for specific operating conditions and should be used in industrial heat pump pilot plant installations. No performance penalty was identified for hydrocarbons compared to synthetic refrigerants, and their use is recommended where possible. Future work should collect more experimental data. In particular, the reduction of the heat transfer coefficient is not yet well understood for high-glide mixtures. Furthermore, hydrocarbon mixtures comprising ethane or hexane would valuably enlarge the pool of available data. Future evaluations should also consider that industrial applications may operate at varying operating conditions throughout the days and seasons. The effects of operation over an array of operating conditions and several dynamic changes should be taken into account when designing mixtures for heat pumps.

Author Contributions: Conceptualization, L.P.M.B.; Funding acquisition, C.A., A.B. and S.N.B.; Investigation, S.N.B.; Project administration, D.R.; Writing—original draft, L.P.M.B.; Writing—review and editing, C.A., D.R., A.B. and S.S.B. All authors have read and agreed to the published version of the manuscript.

Funding: This research received funding from the Swiss National Science Foundation under grant number 203645 and from the Swiss Federal Office of Energy SFOE und project number SI/502260. Their contributions are gratefully acknowledged.

Data Availability Statement: The original contributions presented in the study are included in the article, further inquiries can be directed to the corresponding author.

Conflicts of Interest: The authors declare no conflict of interest.

Nomenclature

Symbols and Abbreviations

ATD	Approach temperature difference	-
<i>a</i>	Coefficients in correlation	various

<i>b</i>	Coefficients in correlation	various
<i>COP</i>	Coefficient of performance	-
Δ	Difference	NA
<i>h</i>	Enthalpy	kJ/kg
<i>HTHP</i>	High temperature heat pump	-
<i>HFC</i>	Hydrofluorocarbon refrigerants	-
<i>HFO/HCFO</i>	Hydrofluoroolefin/Hydrochlorofluoroolefin refrigerants	-
<i>HC</i>	Hydrocarbon refrigerants	-
<i>\dot{m}</i>	Mass flow rate	kg/min
\dot{Q}	Heat transfer rate	kW
ρ	Density	kg/m ³
<i>T</i>	Temperature	°C
<i>UA</i>	UA value	kW/K
<i>V_{swept}</i>	Swept volume	liter
\dot{W}	Compressor power draw	kW
<i>x</i>	Vapor quality or mass fraction	-
Subscripts		
2	State point 2 (compressor outlet)	
60	Dew point temperature of 60 °C	
<i>calc</i>	Calculated	
<i>c or cond</i>	Condenser	
<i>crit</i>	Critical temperature or pressure	
<i>drive</i>	Driving potential	
<i>e or evap</i>	Evaporator	
<i>f</i>	Saturated liquid	
<i>g</i>	Saturated vapor	
<i>gl</i>	Glide	
<i>h</i>	Hot side	
<i>in</i>	Inlet	
<i>IHX</i>	Internal heat exchanger	
<i>meas</i>	Measured	
<i>ois</i>	Overall isentropic	
<i>out</i>	Outlet	
<i>overall</i>	Overall	
<i>r</i>	Ratio	
<i>ref</i>	Refrigerant	
<i>s</i>	Isentropic	
<i>S</i>	Suction state	
<i>si</i>	Sink	
<i>sh</i>	Superheat	
<i>sc</i>	Subcooling	
<i>so</i>	Source	
<i>vol</i>	Volumetric	
<i>w</i>	Water	

Appendix A

Appendix A.1. Temperature Glide of a Mixture

Zeotropic mixtures have a temperature glide, meaning that for some pressure, the saturated vapor temperature is higher than the saturated liquid temperature. This temperature difference becomes smaller towards the critical point and larger as the pressure decreases. It is common practice to speak about “the glide of a mixture” as if it were a constant. In this paper, any reported glide was calculated at the pressure which results in a saturated vapor temperature of 60 °C. Hence:

$$\Delta T_{gl,60} = 60 \text{ }^{\circ}\text{C} - T_{sat,f}(P^*) \quad (\text{A1})$$

$$P^* = P(T_{sat,g} = 60 \text{ }^{\circ}\text{C}) \quad (\text{A2})$$

where $\Delta T_{gl,60}$ is the temperature glide at 60 °C, P^* is the pressure resulting in a saturated vapor temperature of 60 °C and $T_{sat,f}(P^*)$ is the saturated liquid temperature at that pressure.

Appendix A.2. Testing of Flammable Refrigerants

The tested HC refrigerants R-290, R-600, and R-601 are highly flammable (safety category A3). A container was installed outside and equipped with a ventilation system for safe charging and testing of the refrigerants (Figure 4). The 3 × 2 × 2 m (L × W × H) container was designed for up to 6 kg of A3 refrigerants and equipped with an ATEX fan, generating a volumetric flow rate equivalent to at least 10 air exchanges per hour. The air inlet is at the top left front corner of the container. 2/3 of the gas flow exits through the bottom back right corner and 1/3 through the top back right corner. The fan starts operation whenever the light switch is pressed and when 10% of the lower flammability limit is measured by a sensor installed close to the container’s floor. An acoustic signal is emitted when 20% of the flammability limit is reached. In this case, the entire power supply for the container’s interior, except for the ATEX fan, is cut off. The temperature in the container can be controlled with electric resistive heaters to collect data during cold days at ambient temperatures comparable to the lab environment in which other data points were collected.



Figure A1. An outdoor container at OST used to test flammable refrigerants with the laboratory high-temperature heat pump.

Appendix A.3. Separation of COP into Effects of Compressor and Effects of Refrigerant Properties

The COP is a comprehensive and widely used indicator for the system level performance and is strongly dependent on the overall isentropic compressor efficiency as well as the shape of the vapor dome. To understand the influences over a series of measurement data, they can be conveniently separated for a single-stage heat pump as follows:

$$COP = \frac{\dot{Q}_c}{\dot{W}} = \frac{\dot{m} \cdot \Delta h_c}{\frac{\dot{m} \cdot \Delta h_{2s}}{\eta_{ois}}} = \eta_{ois} \cdot \frac{\Delta h_c}{\Delta h_{2s}} \quad (A3)$$

where COP is the coefficient of performance, \dot{Q}_c is the condenser heat transfer rate measured on the refrigerant side, \dot{W} is the compressor power draw, \dot{m} is the refrigerant mass flow rate, Δh_c is the specific enthalpy change of the refrigerant over the condenser, Δh_{2s} is the specific work of the compressor assuming an isentropic and adiabatic compression from a given suction pressure and temperature to a given discharge pressure and η_{ois} is the overall isentropic efficiency. In short:

$$COP = \eta_{ois} \cdot \frac{\Delta h_c}{\Delta h_{2s}} \quad (A4)$$

η_{ois} is the contribution of the compressor at given operating conditions and of course dependent on the suction and discharge pressure, themselves a function also of the heat exchanger geometry. $\Delta h_c / \Delta h_{2s}$ is representative of the thermodynamic properties, capturing the width of the vapor dome and the slope of the isentropes in the P-h diagram.

Appendix A.4. Single Phase Pressure Drop with a Linear Dependence on Mass Flow Rate

Pressure drop for single-phase flow in a pipe can be described as follows:

$$\Delta P = \frac{L f_D \rho u^2}{2D} \quad (A5)$$

ΔP is the pressure drop, L is the length of the pipe, f_D is the Darcy friction factor (four times larger than the Fanning friction factor), ρ is the density of the fluid, u is the flow velocity, D is the pipe diameter. Hence, the pressure drop grows linear with the square of the flow velocity. The mass flow rate is expressed as:

$$\dot{m} = \rho \dot{V} = \rho u A \quad (A6)$$

Rearranging for the flow velocity gives:

$$u = \frac{\dot{m}}{\rho A} \quad (A7)$$

Plugging the formulation for the flow velocity into the equation for the pressure drop gives

$$\Delta P = \frac{L f_D \dot{m}^2}{2D \rho A^2} \quad (A8)$$

In a reciprocating piston compressor, the mass flow rate can be calculated as

$$\dot{m} = f_{Comp} \rho V_{swept} \eta_{vol} \quad (A9)$$

f_{comp} is the compressor frequency (shaft, not electrical), V_{swept} is the total swept volume of all cylinders, and η_{vol} is the volumetric efficiency. Plugging the mass flow rate equation into the pressure drop equation, one obtains

$$\Delta P = \dot{m} \cdot \frac{L f_D f_{Comp} \rho V_{swept} \eta_{vol}}{2D \rho A^2} \quad (A10)$$

And finally

$$\Delta P = \dot{m} \cdot \eta_{vol} \cdot f_D \cdot f_{Comp} \frac{L V_{swept}}{2D A^2} \quad (A11)$$

where everything is a constant but \dot{m} , η_{vol} , f_{comp} and f_D . The compressor frequency f_{comp} was constant throughout the collected data points. The Darcy friction factor f_D is only a function of the wall roughness given high Reynolds numbers. The linear increase

of pressure drop with mass flow rate was to be proven and is shown in Figure 6. The volumetric efficiency varied between experiments and caused the outliers from the linear trend. Assuming f_D and f_{comp} as constant and looking at the ratio of pressure drop to volumetric efficiency:

$$\frac{\Delta P}{\eta_{vol}} = \dot{m} \cdot \frac{f_D f_{Comp} L V_{swept}}{2DA^2} \quad (A12)$$

Figure A2 shows that the correlation is then clear and that data points from synthetic and HC refrigerants both follow the same trend. It is thereby confirmed that there is no significant difference in the friction factor. However, as shown in Figure 6, since the HC refrigerants have a wider vapor dome, their pressure drop for a given heating capacity is smaller.

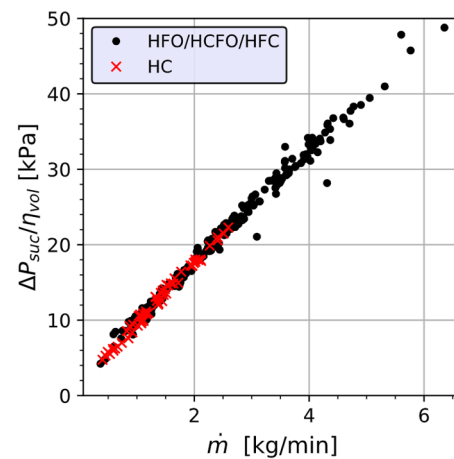


Figure A2. Pressure drop divided by volumetric efficiency as a function of mass flow rate for the suction line.

Appendix A.5. Methods for REFPROP Checks and Composition Determination

The following is a slightly edited explanation from Brendel et al. [25]. Six different methods are proposed to “sanity check” the REFPROP modeling results. For each method, there exists a reference property that can be obtained via a primary and a secondary path. The secondary path always contains a computation of the thermophysical properties of the mixture, which requires the mixture components and mass fractions as inputs. For the liquid phase, density can be measured directly (primary path) but also calculated using temperature, pressure, and mass fractions (secondary path). If the two reference property values obtained via the primary and secondary path are similar, either both the measurement and the prediction are faulty and align coincidentally, or they verify each other as correct. Instead of performing the comparison, all measurements could be assumed to be correct, and the compositions could be declared unknown. Then, there is a mass fraction, which will result in agreement with the reference property values calculated using the primary and secondary path, which can be found iteratively. For this paper, a primary and secondary path was compared and used for composition determination for six different methods.

The primary and secondary path for each method is shown in the Appendix A in Table A1. The symbols in the equations are introduced as follows: T —temperature, P —pressure, x —mass fraction, q —vapor quality, \dot{m} —mass flow rate, \dot{Q} —heat transfer rate, and V —total volume. The subscripts in the equations are introduced as follows: in—inlet, out—outlet, v—valve, e—evaporator (refrigerant side), c—condenser (refrigerant side), si—condenser (water side), equ—equilibrium, hp—heat pump, ref—refrigerant, 1—component one. f_{REF} indicates a REFPROP property call.

Table A1. Mathematical form for composition determination methods.

Name and Functional Form	Primary Path to Reference Property	Secondary Path to Reference Property
	Obtaining property without using REFPROP	Obtaining property using REFPROP
Evaporator inlet temperature ($T_{v,out}$) $x_1 = f(P_{v,out}, T_{v,out}, P_{v,in}, T_{v,in})$ Note: Assume isenthalpic expansion	Direct measurement of $T_{v,out}$	$h_{v,in} = f_{REF}(P_{v,in}, T_{v,in})$ $T_{v,out} = f_{REF}(P_{v,out}, h_{v,in})$
Dewpoint temperature (T_{dew}) $x_1 = f(P_{e,out}, T_{dew}, q = 1)$	Direct measurement of T_{dew}	$T_{dew} = f_{REF}(P_{e,out}, q = 1)$
Density ($\rho_{v,in}$) $x_1 = f(P_{v,in}, T_{v,in}, \rho_{v,in})$	Direct measurement of $\rho_{v,in}$	$\rho_{v,in} = f_{REF}(P_{v,in}, T_{v,in})$
Speed of sound ($u_{v,in}$) $x_1 = f(P_{v,in}, T_{v,in}, u_{v,in})$	Direct measurement of $u_{v,in}$	$u_{v,in} = f_{REF}(P_{v,in}, T_{v,in})$
Condenser heat transfer rate (\dot{Q}_c) $x_1 = f(P_{c,in}, T_{c,in}, P_{c,out}, T_{c,out}, \dot{m}_r, T_{si,in}, T_{si,out}, \dot{m}_{si})$ Note: Assume energy balance closed	$h_{si,out} = f_{REF}(P_{si,out}, T_{si,in})$ $h_{si,in} = f_{REF}(P_{si,in}, T_{si,in})$ $\dot{Q}_c = \dot{m}_{si}(h_{si,out} - h_{si,in})$	$h_{c,in} = f_{REF}(P_{c,in}, T_{c,in})$ $h_{c,out} = f_{REF}(P_{c,out}, T_{c,in})$ $\dot{Q}_c = \dot{m}(h_{c,in} - h_{c,out})$
Resting pressure (P_{equ}) $x_1 = (T_{equ}, P_{equ}, V_{hp}, m_r)$	Direct measurement	$\rho_{tot} = Charge / V_{hp}$ $P_{equ} = f_{REF}(T_{equ}, \rho_{tot})$

Appendix A.6. Overview of Datasets

Table A2. Overview of dataset 1. HFO, HCFO, and HFC refrigerants and mixtures evaluated with a heat pump using compressor A.

Letter	Type	Mixture Components			Charge and Composition			Operating Conditions			Number of Data Points					
		Refrigerant 1	Refrigerant 2	Refrigerant 3	Charge [g]	x_1	x_2	x_3	P_{low} [kPa]	P_{high} [kPa]	Total	with IXH	w/o IXH	DP	RP	Disc.
A	Pure	R-1233zd(E)			4500				52–481	200–2544	26	5	15	5	1	3
E	Pure	R-1336mzz(Z)			4500				48–357	315–1745	31	9	18	3	1	0
H	Pure	R-1234yf			4500				164–984	1149–3168	23	7	13	2	1	8
K	Pure	R-1224yd(Z)			4502				111–384	880–2389	21	9	8	3	1	0
K2	Pure	R-1224yd(Z)			4000				147–258	833–1725	19	12	7	0	0	2
B	Binary	R-1233zd(E)	R-1234yf		5293	0.85	0.15		52–486	482–2609	38	8	25	4	1	8
C	Binary	R-1233zd(E)	R-1234yf		4500	0.7	0.3		104–524	813–2659	29	18	8	3	0	9
D	Binary	R-1233zd(E)	R-1234yf		5727	0.55	0.45		106–602	683–2719	22	7	10	4	1	5
F	Binary	R-1336mzz(Z)	R-1234yf		5000	0.9	0.1		77–437	479–2059	21	10	7	3	1	13
G	Binary	R-1336mzz(Z)	R-1234yf		6000	0.75	0.25		110–546	700–2037	16	11	2	3	0	10
AA	Binary	R-1336mzz(Z)	R-1234yf		3714	0.65	0.35		209–250	1200–1324	4	2	0	1	1	0
AB	Binary	R-1336mzz(Z)	R-1234yf		4010	0.6	0.4		228–270	1286–1419	2	2	0	0	0	0
AC	Binary	R-1336mzz(Z)	R-1234yf		4375	0.55	0.45		251–295	1398–1548	4	2	0	1	1	0
J	Binary	R-1336mzz(Z)	R-1234yf		6000	0.2	0.8		158–809	738–2797	22	10	8	3	1	5
P	Binary	R-1224yd(Z)	R-32		4040	0.99	0.01		157–217	1057–1114	2	2	0	0	0	0
Q	Binary	R-1224yd(Z)	R-32		4124	0.97	0.03		185–245	1150–1231	3	2	0	0	1	0
L	Binary	R-1224yd(Z)	R-32		4739	0.95	0.05		213–293	1245–1381	9	5	0	3	1	2
M	Binary	R-1224yd(Z)	R-32		5002	0.9	0.1		259–352	1628–1867	6	4	0	2	0	1
N	Binary	R-1224yd(Z)	R-32		5424	0.83	0.17		153–584	1717–3122	14	7	4	2	1	5
O	Ternary	R-1224yd(Z)	R-32	R-1336mzz(Z)	6029	0.75	0.15	0.1	190–536	1502–2980	8	5	0	2	1	1
R	Ternary	R-1224yd(Z)	R-32	R-1234yf	4341	0.92	0.03	0.05	206–259	1227–1307	2	2	0	0	0	0
S	Ternary	R-1224yd(Z)	R-32	R-1234yf	4593	0.87	0.03	0.1	223–452	1305–1778	13	8	0	3	2	2
T	Ternary	R-1224yd(Z)	R-32	R-1234yf	4851	0.82	0.03	0.15	240–348	1361–1649	4	3	0	0	1	0
V	Ternary	R-1224yd(Z)	R-32	R-1234yf	5155	0.78	0.02	0.2	256–308	1448–1566	2	2	0	0	0	0

Table A2. Cont.

Letter	Type	Mixture Components			Charge and Composition			Operating Conditions			Number of Data Points					
		Refrigerant 1	Refrigerant 2	Refrigerant 3	Charge [g]	x ₁	x ₂	x ₃	P _{low} [kPa]	P _{high} [kPa]	Total	with IHX	w/o IHX	DP	RP	Disc.
W	Ternary	R-1224yd(Z)	R-32	R-1234yf	5498	0.73	0.02	0.25	272–327	1534–2064	8	2	3	1	2	2
X	Ternary	R-1224yd(Z)	R-32	R-1234yf	5540	0.72	0.03	0.25	278–293	1561–1583	3	3	0	0	0	0
Y	Ternary	R-1224yd(Z)	R-32	R-1234yf	5599	0.71	0.04	0.25	287–295	1639–1661	4	2	0	1	1	0
Z	Ternary	R-1224yd(Z)	R-32	R-1234yf	5718	0.7	0.06	0.24	312–614	1805–2548	9	6	0	2	1	0
AD	Ternary	R-1336mzz(Z)	R-1234yf	R-32	4464	0.54	0.44	0.02	267–310	1531–1692	3	2	0	1	0	0
AE	Ternary	R-1336mzz(Z)	R-1234yf	R-32	4605	0.52	0.43	0.05	197–591	1291–2655	12	7	0	3	2	0
All		R-1336mzz(Z), R-1233zd(E), R-1224yd(Z), R-1234yf, R-32 and mixtures							48–984	200–3168	380	174	128	55	23	76

Table A3. Overview of dataset 2. HFO, HCFO, and HFC refrigerants and mixtures evaluated with a heat pump using compressor B.

Letter	Type	Mixture Components			Charge and Composition			Operating Conditions			Number of Data Points					
		Refrigerant 1	Refrigerant 2	Refrigerant 3	Charge [g]	x ₁	x ₂	x ₃	P _{low} [kPa]	P _{high} [kPa]	Total	with IHX	w/o IHX	DP	RP	Disc.
AN	Pure	R-134a			2500				431–806	867–2689	23	19	4	0	0	0
AH	Pure	R-1224yd(Z)			3503				207–476	1045–1785	13	10	1	1	1	0
AI	Binary	R-1224yd(Z)	R-1234yf		3893	0.90	0.10		254–254	1216–1216	1	1	0	0	0	
AJ	Binary	R-1224yd(Z)	R-1234yf		4379	0.80	0.20		303–303	1422–1422	1	1	0	0	0	
AK	Binary	R-1224yd(Z)	R-1234yf		4671	0.75	0.25		312–528	1514–2447	13	10	2	1	0	
AM	Ternary	R-1224yd(Z)	R-1234yf	R-1336mzz(Z)	5839	0.60	0.20	0.20	165–618	1292–2279	30	25	1	3	1	
All		R-134a, R-1224yd(Z), R-1234yf, R1336mzz(Z) and mixtures							165–806	867–2689	81	66	8	5	2	1

Table A4. Overview of dataset 3. Hydrocarbon refrigerants and mixtures evaluated with a heat pump using compressor B.

Letter	Type	Mixture Components			Charge and Composition			Operating Conditions			Number of Data Points					
		Refrigerant 1	Refrigerant 2	Refrigerant 3	Charge [g]	x ₁	x ₂	x ₃	P _{low} [kPa]	P _{high} [kPa]	Total	with IHX	w/o IHX	DP	RP	Disc.
AP	Pure	R-600			1850				154–535	268–2489	16	8	8	0	0	0
AQ	Binary	R-600	R-290		1947	0.95	0.05		265–265	1406–1406	1	1	0	0	0	
AR	Binary	R-600	R-290		2059	0.90	0.10		293–293	1504–1504	1	1	0	0	0	

Table A4. Cont.

Letter	Type	Mixture Components			Charge and Composition			Operating Conditions			Number of Data Points					
		Refrigerant 1	Refrigerant 2	Refrigerant 3	Charge [g]	x_1	x_2	x_3	P_{low} [kPa]	P_{high} [kPa]	Total	with IHX	w/o IHX	DP	RP	Disc.
AS	Binary	R-600	R-290		2176	0.85	0.15		315–323	1604–1628	2	2	0	0	0	0
AT	Binary	R-600	R-290		2312	0.80	0.20		150–683	416–2204	15	8	5	1	1	0
AU	Binary	R-600	R-290		2642	0.70	0.30		407–407	1951–1951	1	1	0	0	0	0
AV	Binary	R-600	R-290		3083	0.60	0.40		452–452	2156–2156	1	1	0	0	0	0
AW	Binary	R-600	R-290		3524	0.52	0.48		512–512	2332–2332	1	1	0	0	0	0
BF	Binary	R-600	R-290		1857	0.35	0.65		642–642	2622–2622	1	1	0	0	0	0
BG	Binary	R-600	R-290		2172	0.30	0.70		642–642	2721–2721	1	1	0	0	0	0
BH	Binary	R-600	R-290		2600	0.25	0.75		655–655	2828–2828	1	1	0	0	0	0
BI	Binary	R-600	R-290		3250	0.20	0.80		626–730	629–3104	2	1	0	0	1	0
AX	Binary	R-601	R-290		1587	0.70	0.30		232–232	1310–1310	1	1	0	0	0	0
AY	Binary	R-601	R-290		1845	0.60	0.40		304–304	1630–1630	1	1	0	0	0	0
AZ	Binary	R-601	R-290		2214	0.50	0.50		311–458	1654–2730	9	7	1	1	0	0
BA	Binary	R-601	R-290		2575	0.43	0.57		464–464	2162–2162	1	1	0	0	0	0
BB	Binary	R-601	R-290		3163	0.35	0.65		543–543	2342–2342	1	1	0	0	0	0
BC	Binary	R-601	R-290		2427	0.3	0.7		474–724	1331–2893	4	4	0	0	0	0
BD	Binary	R-601	R-290		2231	0.2	0.8		309–645	2069–2723	2	1	1	0	0	0
BE	Binary	R-601	R-290		2973	0.15	0.85		685–685	2967–2967	1	1	0	0	0	0
All									150–730	268–3104	63	44	15	2	2	0

Appendix A.7. Deviation of Measured and Calculated Property for Each Method

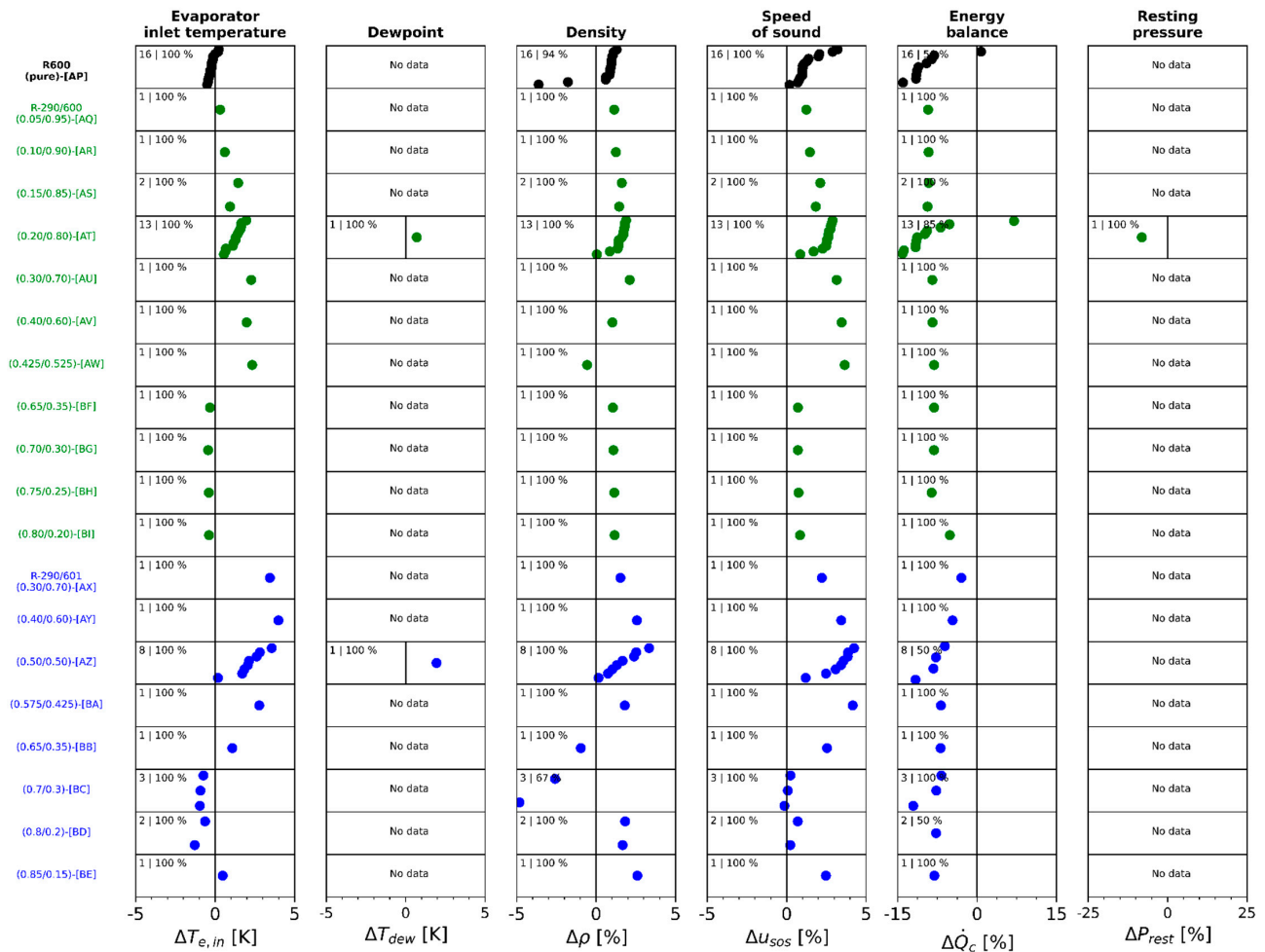


Figure A3. Deviation of directly measured properties and values calculated from REFPROP for pure butane and all tested hydrocarbon mixtures. The color black represents pure fluids. The color green was assigned to the propane/butane mixture. Blue was assigned to the propane/pentane mixture.

Appendix A.8. Approach Temperature Difference

The approach temperature difference is defined here as the smallest temperature difference occurring between two fluids in a heat exchanger. In an evaporator, the approach temperature difference can only occur at either end of the heat exchanger. The temperatures of both fluids here are known from measurements. In a condenser, the approach temperature could occur at the end of the heat exchanger where the refrigerant is subcooled or at the point where the refrigerant is a saturated vapor.

Appendix A.9. Evaporator Correlation

Data points with an ATD of less than 1.5 K ($\Delta T_{so} / \Delta T_{sh,e,out} < 1$) are assigned an approach temperature of 1 K by default in the proposed correlation. These data points, therefore, do not need to be approximated by the fitted correlation, which simplifies the correlation design. The data points are still shown in Figure A4 (right) with small black crosses. The correlation, as defined in Equation REF, is shown along with the data in Figure A4 (right).

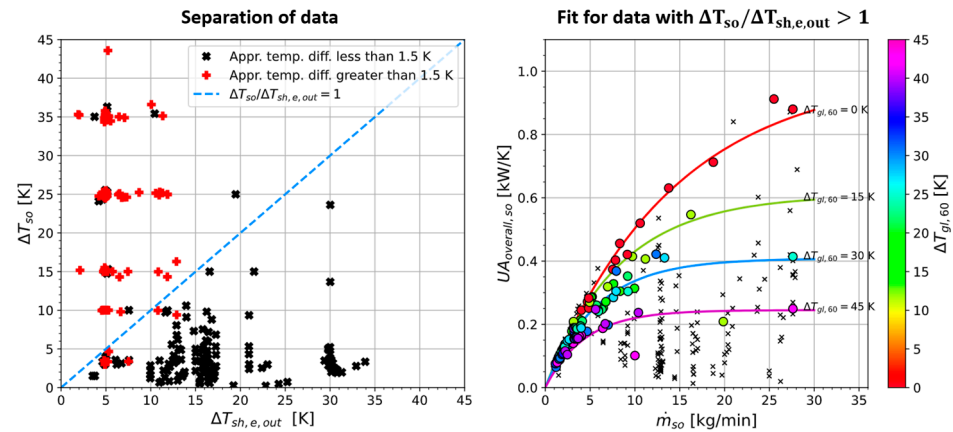


Figure A4. Visualization of evaporator data split (left) and UA value correlation (right). Figure from Brendel et al. [37]. In the right hand side figure, colored circles represent the data with approach temperature differences greater than 1.5 K which must be fitted by the correlation (red “+”-markers in the left hand side figure). Small black x-markers represent data which can be assigned a 1 K approach temperature difference (black x-markers in the left-hand side figure) and must not be covered by the correlation.

Appendix A.10. Condenser Correlation

The condenser correlation divides the data into three groups. All data for which $\Delta T_{si} > 15$ K is shown with colored markers in Figure A5 (left) with lines showing the correlation as in equation REF. All data for which $\Delta T_{si} < 15$ K is shown as small x markers. Figure A5 (right) shows only data for which $\Delta T_{si} < 15$ K. Of this group, any data points with $\Delta T_{gl,60} < 5$ K is assigned an ATD of 1 K and shown with small black x-markers. The remaining data is fitted with the correlation as in Equation REF

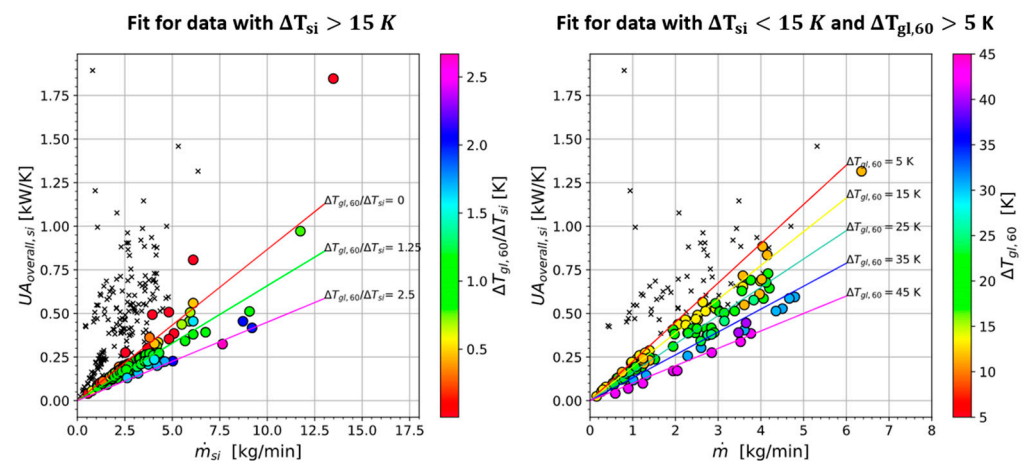


Figure A5. Visualization of condenser UA value correlation for $\Delta T_{si} > 15$ K (left) and $\Delta T_{si} < 15$ K with $\Delta T_{gl,60} > 5$ K (right). Figure from Brendel et al. [37]. Colorized circles represent the data with approach temperature differences greater than 1.5 K which must be fitted by the correlation. Small black x-markers represent data which can be assigned a 1 K approach temperature difference and must not be covered by the correlation.

References

1. McLinden, M.O.; Radermacher, R. Methods for comparing the performance of pure and mixed refrigerants in the vapour compression cycle. *Int. J. Refrig.* **1987**, *10*, 318–325. [CrossRef]
2. Azzolin, M.; Berto, A.; Bortolin, S.; Col, D.D. Two-Phase Heat Transfer of Low GWP Ternary Mixtures. In Proceedings of the Purdue Conferences, West Lafayette, IN, USA, 24–28 May 2021.
3. Cavallini, A.; Censi, G.; Del Col, D.; Doretto, L.; Longo, G.A.; Rossetto, L. Condensation of Halogenated Refrigerants Inside Smooth Tubes. *HVACR Res.* **2002**, *8*, 429–451. [CrossRef]

4. Fronk, B.M.; Garimella, S. In-tube condensation of zeotropic fluid mixtures: A review. *Int. J. Refrig.* **2013**, *36*, 534–561. [CrossRef]
5. Granryd, E.; Ekroth, I.; Lundqvist, P.; Melinder, A.; Palm, B.; Rohlin, P. *Refrigeration Engineering*; Royal Institute of Technology: Stockholm, Sweden, 2009.
6. Jige, D.; Nobunaga, M.; Nogami, T.; Inoue, N. Condensation heat transfer of refrigerant mixtures of R1234yf and R32 in multiport minichannels. In Proceedings of the 26th International Congress of Refrigeration, Paris, France, 21–25 August 2023.
7. Jige, D.; Nobunaga, M.; Nogami, T.; Inoue, N. Boiling heat transfer of binary and ternary mixtures in multiple rectangular microchannels. *Appl. Therm. Eng.* **2023**, *229*, 120613. [CrossRef]
8. Radermacher, R.; Hwang, Y. *Vapor Compression Heat Pumps with Refrigerant Mixtures*, 1st ed.; CRC Press: Boca Raton, FL, USA, 2005.
9. Brendel, L.P.M.; Bernal, S.N.; Widmaier, P.; Roskosch, D.; Bardow, A.; Bertsch, S.S. High-Glide Refrigerant Blends in High-Temperature Heat Pumps: Part 1—Coefficient of Performance. *Int. J. Refrig.* **2024**; *publication in progress*.
10. Granryd, E. Hydrocarbons as refrigerants—An overview. *Int. J. Refrig.* **2001**, *24*, 15–24. [CrossRef]
11. Kim, J.H.; Cho, J.M.; Kim, M.S. Cooling performance of several CO₂/propane mixtures and glide matching with secondary heat transfer fluid. *Int. J. Refrig.* **2008**, *31*, 800–806. [CrossRef]
12. Mohanraj, M.; Jayaraj, S.; Muraleedharan, C.; Chandrasekar, P. Experimental investigation of R290/R600a mixture as an alternative to R134a in a domestic refrigerator. *Int. J. Therm. Sci.* **2009**, *48*, 1036–1042. [CrossRef]
13. Quenel, J.; Anders, M.; Atakan, B. Propane-isobutane mixtures in heat pumps with higher temperature lift: An experimental investigation. *Therm. Sci. Eng. Prog.* **2023**, *42*, 101907. [CrossRef]
14. Venzik, V.; Roskosch, D.; Atakan, B. Propan/Isobutan-Gemische als alternative Kältemittel in Kompressionskältemaschinen: Eine experimentelle Untersuchung. *Forsch. Ingenieurwesen* **2020**, *84*, 65–77. [CrossRef]
15. Venzik, V.; Roskosch, D.; Atakan, B. Propene/isobutane mixtures in heat pumps: An experimental investigation. *Int. J. Refrig.* **2017**, *76*, 84–96. [CrossRef]
16. Wongwises, S.; Kamboon, A.; Orachon, B. Experimental investigation of hydrocarbon mixtures to replace HFC-134a in an automotive air conditioning system. *Energy Convers. Manag.* **2006**, *47*, 1644–1659. [CrossRef]
17. Wongwises, S.; Chimres, N. Experimental study of hydrocarbon mixtures to replace HFC-134a in a domestic refrigerator. *Energy Convers. Manag.* **2005**, *46*, 85–100. [CrossRef]
18. Luo, J.; Yang, K.; Liu, Y.; Zhao, Z.; Chen, G.; Wang, Q. Experimental and theoretical assessments on the systematic performance of a single-stage air-source heat pump using ternary mixture in cold regions. *Appl. Therm. Eng.* **2023**, *234*, 121300. [CrossRef]
19. Luo, J.; Wang, Q.; Yang, K.; Zhao, Z.; Chen, G.; Zhang, S. Performance investigation on a novel air-source heat pump using CO₂/HC for recirculated water heater in cold regions. *Sustain. Energy Technol. Assess.* **2022**, *53*, 102496. [CrossRef]
20. Brendel, L.P.M.; Bernal, S.N.; Arpagaus, C.; Roskosch, D.; Bardow, A.; Bertsch, S.S. Experimental investigation of high-glide refrigerant mixture R1233zd(E)/R1234yf in a high-temperature heat pump. In Proceedings of the International Congress of Refrigeration, Paris, France, 21–25 August 2023.
21. Brendel, L.P.M.; Bernal, S.N.; Roskosch, D.; Arpagaus, C.; Bertsch, S.S. Compressor performance for varying compositions of high-glide mixtures R1233zd(E)/R1234yf and R1336mzz(Z)/R1234yf. In Proceedings of the 13th International Conference on Compressors and their Systems, London, UK, 11–13 September 2023. [CrossRef]
22. Arpagaus, C.; Bless, F.; Uhlmann, M.; Büchel, E.; Frei, S. High temperature heat pump using HFO and HCFO refrigerants—System design, simulation, and first experimental results. In Proceedings of the Purdue Conferences, West Lafayette, IN, USA, 9–12 July 2018; Available online: <https://docs.lib.purdue.edu/iracc/1875/> (accessed on 21 November 2023).
23. Fuchs, “Reniso Triton SE170”, Fuchs Lubricants Germany GmbH. Available online: <https://www.fuchs.com/de/en/product/product/148791-RENISO-TRITON-SE-170/> (accessed on 21 November 2023).
24. Fuchs, “Reniso Triton LPG150”, Fuchs Lubricants Germany GmbH. Available online: <https://www.fuchs.com/de/en/product/product/151011-RENISO-LPG-150/> (accessed on 21 November 2023).
25. Brendel, L.P.M.; Bernal, S.N.; Hemprich, C.; Rowane, A.J.; Bell, I.H.; Roskosch, D.; Arpagaus, C.; Bardow, A.; Bertsch, S.S. High-Glide Refrigerant Blends in High-Temperature Heat Pumps: Part 2—Inline Composition Determination for Binary Mixtures. *Int. J. Refrig.* **2024**; *publication in progress*.
26. Brendel, L.P.M.; Wördemann, M.; Bernal, S.; Arpagaus, C.; Bertsch, S.S. High-glide refrigerant mixtures for HTHPs with different temperature changes on the heat sink and heat source. In Proceedings of the HTHP Symposium, Copenhagen, Denmark, 23–24 January 2024.
27. Lemmon, E.W.; McLinden, M.O.; Wagner, W. Thermodynamic Properties of Propane. III. A Reference Equation of State for Temperatures from the Melting Line to 650 K and Pressures up to 1000 MPa. *J. Chem. Eng. Data* **2009**, *54*, 3141–3180. [CrossRef]
28. Bücker, D.; Wagner, W. Reference Equations of State for the Thermodynamic Properties of Fluid Phase n-Butane and Isobutane. *J. Phys. Chem. Ref. Data* **2006**, *35*, 929–1019. [CrossRef]
29. Thol, M.; Uhde, T.; Lemmon, E.W.; Span, R. Fundamental Equations of State for Hydrocarbons. Part I. *Fluid Phase Equilibria*. 2019. Available online: http://www.coolprop.org/fluid_properties/fluids/n-Pentane.html (accessed on 21 November 2023).
30. Tillner-Roth, R.; Yokozeki, A. An International Standard Equation of State for Difluoromethane (R-32) for Temperatures from the Triple Point at 136.34 K to 435 K and Pressures up to 70 MPa. *J. Phys. Chem. Ref. Data* **1997**, *26*, 1273–1328. [CrossRef]
31. Tillner-Roth, R.; Baehr, H.D. A International Standard Formulation for the Thermodynamic Properties of 1,1,1,2-Tetrafluoroethane (HFC-134a) for Temperatures from 170 K to 455 K and Pressures up to 70 MPa. *J. Phys. Chem. Ref. Data* **1994**, *23*, 657–729. [CrossRef]

32. Lemmon, E.W.; Akasaka, R. An International Standard Formulation for 2,3,3,3-Tetrafluoroprop-1-ene (R1234yf) Covering Temperatures from the Triple Point Temperature to 410 K and Pressures Up to 100 MPa. *Int. J. Thermophys.* **2022**, *43*, 119. [[CrossRef](#)]
33. Akasaka, R.; Fukushima, M.; Lemmon, E.W. A Helmholtz Energy Equation of State for cis-1-chloro-2,3,3,3-Tetrafluoropropene (R-1224yd(Z)). In Proceedings of the European Conference on Thermophysical Properties, Graz, Austria, 3–8 September 2017.
34. Mondéjar, M.E.; McLinden, M.O.; Lemmon, E.W. Thermodynamic Properties of trans-1-Chloro-3,3,3-trifluoropropene (R1233zd(E)): Vapor Pressure, (p , ρ , T) Behavior, and Speed of Sound Measurements, and Equation of State. *J. Chem. Eng. Data* **2015**, *60*, 2477–2489. [[CrossRef](#)]
35. McLinden, M.O.; Akasaka, R. Thermodynamic Properties of cis-1,1,1,4,4,4-Hexafluorobutene [R-1336mzz(Z)]: Vapor Pressure, (p , ρ , T) Behavior, and Speed of Sound Measurements and Equation of State. *J. Chem. Eng. Data* **2020**, *65*, 4201–4214. [[CrossRef](#)]
36. Doughty, O.; Arpagaus, C.; Bertsch, S.S.; Brendel, L.P.M. Set of Performance Correlations for Reciprocating Compressor Covering Synthetic and Hydrocarbon Refrigerants. In Proceedings of the Purdue Conferences, West Lafayette, IN, USA; 2024. *under review*.
37. Brendel, L.P.M.; Arpagaus, C.; Roskosch, D.; Bertsch, S.S. High-glide ternary mixtures in high-temperature heat pumps. In Proceedings of the DKV Tagung, Hannover, Germany, 22–24 November 2023.

Disclaimer/Publisher’s Note: The statements, opinions and data contained in all publications are solely those of the individual author(s) and contributor(s) and not of MDPI and/or the editor(s). MDPI and/or the editor(s) disclaim responsibility for any injury to people or property resulting from any ideas, methods, instructions or products referred to in the content.